EFFECTS OF NORMAL AND EXTREME ENVIRONMENT ON REINFORCED CONCRETE STRUCTURES

by

BORIS BRESLER

Professor of Civil Engineering
Department of Civil Engineering
University of California
Berkeley, California

ROBERT H. IDING

Lecturer
School of Architecture
California Polytechnic State University
San Luis Obispo, California

Report No. UC SESM 77-4
Structural Engineering and Structural Mechanics
Department of Civil Engineering
University of California
Berkeley, California

May 1977

EFFECTS OF NORMAL AND EXTREME ENVIRONMENT ON REINFORCED CONCRETE STRUCTURES was presented at the Douglas McHenry International Symposium on Concrete and Concrete Structures held in Mexico City during the ACI-IMCYC Fall Convention in October 1976. The paper has been accepted for publication by the American Concrete Institute in the Douglas McHenry Symposium Volume and is reproduced here by permission of the ACI.

SYNOPSIS

Prediction of the response of reinforced concrete structures to variations in temperature, humidity, and load is described. Modeling of structures, loading history, environment, and material behavior is discussed and several case studies are included to illustrate the use of proposed models. The models account for nonlinear behavior under variations in load and environment and for the nonhomogeneity introduced by steel reinforcement and cracking of concrete.

TABLE OF CONTENTS

TABLE OF CONTENTS (cont.)

INTRODUCTION

Cracking, excessive deformation, spalling, and even partial collapse of reinforced concrete structures frequently result from variations in environmental and loading conditions not considered in design. Such distress should be minimized by using analyses of the effects of complex environmental and loading histories in design practice.

A general scheme for such a design process is illustrated in the flow chart in Fig. 1 where the sequence of evaluation and analysis is indicated. Basically, one must: (1) model the structure, (2) model environmental and loading histories, (3) decide whether an environmental response analysis is required, (4) execute an environmental response analysis when necessary; otherwise, proceed directly to structural response analysis, (5) analyze structural response to critical loading combinations, including environmental effects when necessary, and (6) verify that structural response complies with performance requirements.

Structural response can be closely approximated if the following are accounted for:

(1) stress-related instantaneous and creep deformation as well as dimensional changes caused by temperature or shrinkage variations;

(2) changes in mechanical properties of materials with age, temperature, and humidity; and

(3) degradation in local cross sections through cracking and crushing in concrete, and/or through yielding of steel.

The simplified models for selected environments and for material behavior described in this paper permit practical engineering solutions. Nonuniform moisture and heat flow effects -- shrinkage and temperature

changes -- are modeled using nonlinear diffusion equations and boundary conditions. Free volume changes associated with shrinkage and thermal changes are calculated independently of stress effects assuming that stresses, cracking, and other structural behavior do not affect moisture flow. Predictions of free volume change serve as input for structural analyses. Structural effects, including stresses, deformations, cracking, crushing, and yielding, are calculated using a nonlinear stiffness method based on a simplified finite element approach. Continuously varying processes are modeled using time step integration. Several case studies are presented to illustrate the general approach described in this paper.

MODELING THE STRUCTURE

To simplify structural analysis and determination of thermal and shrinkage distribution throughout a concrete structure, large structures are substructured, substructures are divided into members, members are divided into segments, and segments are divided into elements representing concrete and steel components.

A typical idealization of a reinforced concrete frame is shown in Fig. 2. Within each segment, elementary beam theory is enforced, i.e., plane sections remain plane, and moment along the axis of a beam segment is assumed to vary linearly. Cross-sectional geometry and material properties are assumed to be constant within each segment during a specified time interval.

Since element mesh size and shape strongly influence the efficiency and accuracy of finite element analyses, the following factors should be considered when devising a mesh:

(1) Computational effort increases rapidly with number of elements. Therefore, symmetry should be taken advantage of wherever possible to reduce the portion of a structure or element to be analyzed.

(2) Small elements should be used where significant thermal and shrinkage gradients and degradation of cross sections may be expected.

(3) Nodes should be numbered so as to minimize the bandwidth of resulting matrix equations, thereby decreasing computational effort.

Time step size will vary depending on environmental and loading histories. Accuracy generally increases with smaller time steps, but so does computational effort and cost. Small time steps are needed when environmental conditions, material properties, or response characteristics change rapidly since high rates of change in thermal or drying shrinkage result in high rates of change in stress state or material degradation. Sudden discontinuities, such as cracking or crushing, also require smaller time steps to avoid convergence difficulties in numerical calculation.

LOADING HISTORY

Important variations in loading during the life of a structure include the following stages.

Construction Stage

Load increments during the construction stage include increments due to placement of concrete (precast or cast-in-place), removal of form shoring and other temporary bracing, special construction equipment (cranes, elevators), storage of nonstructural elements prior to

installation, and to prestressing carried out in stages. In some cases the effect of wind loads on a structure before the lateral force-resisting system is completed may be important and must be considered when precast construction is used, although the significance of this condition would depend on construction sequence.

The influence of early load history on structural response is particularly important when large loading increments develop while concrete is not fully mature, and when loading effects occur while modulus of elasticity and tensile strength are relatively low and/or specific creep is high. Early age loading may also combine with environmental effects and result in substantial stress and deformation at the end of the construction stage before a structure is subjected to any service load.

Service Life Stage

During the life of a structure, load increments are due to furnishing and occupancy loads in buildings, traffic loads on bridges, buoyancy loads on floating structures, storm (wind or wave) action on stationary or floating structures, and hazard loads such as earthquakes or explosive loads. In addition to variations in external loading history, the possibility of changes in support conditions, such as foundation settlement, may have to be considered as part of the loading history during this stage.

MODELING THE ENVIRONMENT

Physical environmental effects can be divided into two categories: normal service and extreme conditions. In the first category, local atmospheric environment predominates for ordinary structures. For some

structures, normal service environment may involve exposure to special thermal conditions. Environmental conditions likely to produce corrosion or other material deterioration must also be considered.

In the second category -- extreme environmental conditions -- the effects of storms (including tornadoes and hurricanes), floods, earthquakes, fires, and other extreme exposures must be considered. Because of space limitations, only models for atmospheric environment and fire environment will be discussed here.

Atmospheric Environment

Structural response to changes in environment depends on variations in ambient air temperature, relative humidity, wind, and sky cover. The latter influences the radiation component of heat transfer to or from exterior surfaces of structures. In addition, the amount of daily precipitation may be important as well as accumulated snow pack on structures. Data on weather conditions are compiled at U.S. weather stations and published by the U.S. Department of Commerce, NOAA, Environmental Data Service, Climatological Data Reports. Relevant data may vary; in some cases, variations in daily temperature for a specified period of time may be important (Fig. 3), while in other cases, extreme temperature (lows and highs) with a specified return period or a specified probability of occurrence [1] may be important (Fig. 4). Modeling meteorological parameters may be particularly important in evaluating the response of bridge decks and pavement systems [2].

Boundary conditions for exterior concrete walls or roofs must account for both convective and radiative heat transfer, representing conditions such as those shown in Fig. 5a. Mackey and Wright [3] have proposed using equivalent air temperatures, compensated for radiation

conditions (Fig. 5b), so that only convection boundary conditions need be used with these air temperatures (Fig. 5c).

Atmospheric conditions also affect moisture movement within structural elements. Relative humidity and temperature influence both total moisture loss and speed of the diffusion process [4].

Fire Environment Modeling

Fire environment models must be selected so as to permit calculation of the thermal response of a structure to fire, requiring that actual fire conditions in a compartment be simplified considerably. Problems related to describing compartment fires have been examined by several investigators [5-8]. All studies indicate that the standard ASTM E-119 curve is inadequate for predicting structural response to fire. The important parameters in establishing models for fire environment are fire load, ventilation, compartment geometry, and surface characteristics [6,7]. Given these parameters, it should be possible to establish time-temperature characteristics of a pseudo-fire, represented by a well-mixed, turbulent, continuous gas flame in all or part of a compartment. In addition, effective emissivity of a compartment fire should be defined so that appropriate radiation boundary conditions can be used to calculate temperature histories within structural elements.

A typical pseudo-fire time-temperature curve is shown in Fig. 6. A continuous time-temperature curve may be idealized by multilinear segments representing periods of: (a) rapid development of a fully involved fire, (b) maximum temperature and duration of a fully involved fire, and (c) decay of a fully involved fire (Fig. 7). These phases must be included in a fire environment model because different phases may govern the response of different structures. A multilinear pseudo-fire model may be

defined by four characteristic times (t_1, t_2, t_3, and t_4) and three characteristic temperature rates ($\dot{T}_1$, $\dot{T}_2$, and $\dot{T}_3$). Typical ranges for these values are shown in Table 1. Values for these ranges will vary for individual fires depending on combustible content (fire load), ventilation, etc. For design purposes, however, it may be possible to reduce fire environment models to four basic types as shown in Fig. 8.

MODELING MATERIAL BEHAVIOR

To predict overall structural response, the material characteristics determining response to loading history and to changes in environment must be modeled. In the structural response analysis proposed here, two types of strains are calculated: (1) 'free' strains associated with changes in the environment in the absence of any restraint or stress, and (2) stress-related strains (instantaneous and time-dependent) including degradation of material such as cracking or crushing of concrete.

For any time increment Δt, overall change in strain increment, $\Delta\varepsilon$, can be divided into the following components:

$$\Delta\varepsilon = \text{(free strain increment + stress-related strain increment)}$$
$$= (\Delta\varepsilon_T + \Delta\varepsilon_S) + (\Delta\varepsilon_C + \Delta\varepsilon_\sigma) \quad (1)$$

where $\Delta\varepsilon_T$ is thermal strain increment, $\Delta\varepsilon_S$ is free shrinkage strain increment, $\Delta\varepsilon_C$ is creep or any other imposed strain increment (such as aging, foundation settlement, etc.), and $\Delta\varepsilon_\sigma$ is instantaneous strain increment due to stress change $\Delta\sigma$ under specified environmental conditions. Values of $\Delta\sigma$ are calculated from equilibrium conditions so that overall deformation satisfies compatibility conditions, and strain increments $\Delta\varepsilon$ satisfy stress-strain laws and failure criteria.

Free Strain Increments

Thermal strain -- During time interval Δt thermal strain increment $\Delta\varepsilon_T(t)$ is proportional to temperature increment ΔT, i.e.

$$\Delta\varepsilon_T(t) = \alpha(T)\Delta T(t) \tag{2}$$

where $\alpha(T)$ is a temperature-dependent coefficient of thermal expansion or contraction, and $\Delta T(t)$ is the increment in temperature $T(t)$. Values of $T(t)$ can be obtained by solving the heat diffusion equation using appropriate models for thermal properties of the material and boundary conditions. Ranges of variation of coefficients of thermal expansion with temperature for steel and concrete are shown in Fig. 9.

Shrinkage strain -- The concrete free shrinkage strain increment $\Delta\varepsilon_S(t)$ may be assumed to be proportional to moisture change so that

$$\Delta\varepsilon_S(t) = k(M)\cdot\Delta M \tag{3}$$

where $k(M)$ is a moisture-dependent coefficient of shrinkage or swelling and ΔM is moisture change. To determine variations in $k(M)$ and moisture change ΔM, complex physico-chemical processes (see Refs. 9-13) must be considered. Usually, it is sufficiently accurate to assume that shrinkage or swelling can be modeled directly by a diffusion process without precisely determining $k(M)$ or ΔM, and that

$$\Delta\varepsilon_S(t) = \Delta S(t) \tag{4}$$

where $S(t)$ is a stress-independent (free) dimensional change determined by solving the shrinkage diffusion equation using appropriate models for shrinkage properties of the material and boundary conditions as described in the following section.

Stress-Related Strain Components

Stress-related strain consists of two components, one due to instantaneous and the other to creep strain.

Instantaneous strains -- For the general case considered here, a nonlinear stress-strain relationship is used which represents an instantaneous response of a material loaded in tension or compression. For materials having an initially linear elastic range, the stress-strain relationship is independent of stress history as long as prior maximum stress does not exceed elastic limit. For the general nonlinear case, it is necessary to describe unloading and reloading behavior in terms of the initial loading curve.

Steel -- For steel in either tension or compression, once elastic limit has been exceeded, unloading and reloading within a specified stress range follow elastic behavior. Outside the specified stress range -- approximately equal to twice the elastic limit -- loading follows the same law as initial loading, while unloading is always elastic. This model, generally accepted for steel, is shown in Fig. 10.

Concrete -- For concrete in compression, the model is similar to that for steel, except that it generally has no linear portion. Unloading is assumed to be elastic, following a linear stress-strain path with a slope equal to the initial modulus of the material. On reloading, behavior is linearly elastic following the preceding unloading path up to the stress limit defined by the initial loading curve. Beyond this point, the stress-strain relationship of initial loading governs up to a specified value of ultimate strain ε_U at which time concrete is assumed to be 'crushed' and unable to resist stress. This relationship is shown in Fig. 11.

For concrete in tension, the stress-strain law is more difficult to define because the extensibility of reinforced concrete is greater than that of plain concrete [14,16]. In general, concrete properties in tension (in the presence of reinforcing steel) may be represented by a curve with an ascending and a descending branch, similar to that for compression (Fig. 11).

When maximum tensile strain exceeds elastic limit, unloading follows a linear path which is directed towards the origin, i.e., no residual inelastic strain is allowed in tension. Reloading follows the same linear unloading path until a point on the basic stress-strain curve is reached. This curve then controls as tensile strain increases to some specified ultimate value. Concrete is assumed to crack at this ultimate strain and thereafter to be unable to resist tension. However, with load reversal, when prior extension is reversed, cracks close and concrete is capable of resisting compression. In this analysis, it is assumed that prior cracking does not impair the ability of concrete to resist compression, but that cracking precludes concrete from resisting tension under any subsequent loading. The basic stress-strain relationship for concrete under uniaxial compression or tension stress histories is shown in Fig. 11.

Effect of temperature on instantaneous strain -- The influence of elevated temperature on the nonlinear stress-strain characteristics of steel and concrete has not been established conclusively by experimentation. Effects of constant elevated temperature on basic stress-strain characteristics have been investigated for some structural steels in tension and for some concretes in compression. However, combined effects of varying temperature and loading condition have not been fully investigated.

Recent studies on concrete at elevated temperature by Anderberg and Thelandersson [17] suggest that effects of stress history and temperature

history may be important. In this paper, it is assumed that for concrete subjected to nominal compression during heating, the compression stress-strain characteristics of concrete at elevated temperature are independent of previous stress or temperature history. The model for compression stress-strain diagrams used in this analysis is based on Furumura's results [18], while the model for tension diagrams is based on the hypothesis that the nondimensional ratios (σ/f_t) and $(\varepsilon/\varepsilon_t)$ are independent of temperature. The resulting variation of steel and concrete stress-strain diagrams with temperature is shown in Figs. 12 and 13.

Creep strain -- General creep strain formulations use the superposition principle with appropriate modifications for aging, temperature effect, and nonlinear effects at high stress levels. Creep of reinforcing steel at normal ambient temperature is negligible. For concrete, the general expression for creep strain increment due to stress increment $\Delta\sigma_i$ is

$$\Delta\varepsilon_{cj}^{cr} = C_j(H_j^n)\Delta\sigma_j \tag{5}$$

where $C_j(H_j^n)$ is a specific creep coefficient determined for a specified time interval and temperature history. For concrete at a constant temperature, the specific creep function may be expressed as follows:

$$C_j(T,\tau) = A_j(\tau)\ \Sigma\ [1 - e^{-k_i(T-\tau)}] \tag{6}$$

where $A_j(\tau)$ is a function to account for the effect of aging, τ is age at loading, k_i are coefficients related to retardation times for a particular concrete, T is age at observation of strain, and $(T-\tau)$ is duration of loading.

When the effects of aging on instantaneous deformation and on creep deformation within linear stress-strain range are combined, the strain increment $\Delta\varepsilon_{cj}$ may be expressed as follows:

$$\Delta\varepsilon_{cj} = \Delta\varepsilon_{cj}^{inst} + \Delta\varepsilon_{cj}^{cr} = [\frac{1}{E_{cj}(\tau)} + C_j(H_j^n)]\Delta\sigma_j \qquad (7)$$

A typical compliance surface showing the effect of aging on instantaneous and creep strains is shown in Fig. 14.

For stresses in excess of about 40% of compressive strength, the definition of strain increment is more complex as $\Delta\varepsilon_{cj}^{inst}$ becomes a nonlinear function of stress intensity and history, and $\Delta\varepsilon_{cj}^{cr}$ becomes a function of amplified effective stress increment [19].

Although specific creep for concrete in compression may differ from that for tension, the two may be assumed equal as a first order approximation.

Effect of temperature on creep strain -- The effect of elevated temperature on creep strain can be modeled using temperature-compensated time that reflects amplification of creep with temperature. Appropriate time-temperature shift functions must be developed from experimental data for particular reinforcing steels and concrete mixes; modified shift functions can also account for aging [20-23].

At elevated temperature, creep in reinforcing steel is significant, and creep at variable elevated temperature and stress is usually modeled by a combination of temperature-compensated time according to Sherby and Dorn [24] and a strain-hardening rule wherein temperature-compensated variable time and a stress-dependent coefficient are derived from experimental data. Modifications of Harmathy's expressions [25] have been used in the present study. It must be emphasized that creep rate can be

highly sensitive to derived coefficients, and for steels characterized by different yield strengths, plastic plateaus, and strain-hardening behavior, coefficients for steel creep at elevated temperature may vary widely.

Creep strain increments $\Delta\varepsilon_c$ during a specified time step are calculated using the models outlined above. For convenience in numerical analysis, these strain increments are then included with free strain components.

MODELING FREE VOLUME CHANGES

The first step in analyzing environmental response is to determine unrestrained free volume change due to moisture movement (shrinkage) and temperature change. Both types of volume change are essentially transient diffusion processes and can be modeled by a differential equation of the type:

$$K \nabla^2 U + Q = C \frac{\partial U}{\partial t} \qquad (8)$$

Equation 8 is a balance law that controls heat flow or shrinkage development (variable U) at every point in a structure, and at all times in its response history. When material characteristics are defined by coefficients K and C and combined with internal or external flow conditions Q, the diffusion equation can be solved to determine temperature or shrinkage history within a structure.

The physical meaning of the diffusion equation can be expressed simply as follows:

RATE AT WHICH HEAT OR SHRINKAGE FLOWS FROM ELEMENTS ADJACENT TO A NODE (POINT)	+	RATE AT WHICH HEAT OR SHRINKAGE ENTERS ELEMENTS ADJACENT TO A NODE (POINT)	=	RATE AT WHICH HEAT OR SHRINKAGE IS STORED (INCREASES) IN ELEMENTS ADJACENT TO A NODE (POINT)

Thermal Volume Changes

For heat flow, the diffusion equation takes the well-known form

$$K\left(\frac{\partial^2 T}{\partial x^2} + \frac{\partial^2 T}{\partial y^2}\right) + Q = \rho C \frac{\partial T}{\partial t} \tag{9}$$

where x and y are point coordinates in a two-dimensional space, T is temperature, and t is time. This equation is derived from elementary thermodynamic principles and states that heat stored in an element of material ($\rho C \cdot \partial T/\partial t$) must equal heat flowing into that element from adjacent parts of a structure ($K \cdot \nabla^2 T$) combined with heat generated within an element (Q). The thermal properties of a material are characterized by three parameters: K (conductivity - a measure of time rate of heat conduction per unit difference in temperature), C (heat capacity - a measure of quantity of heat necessary to produce unit change of temperature in unit mass), and ρ (density). The first two material parameters are temperature dependent; typical ranges of values are shown in Figs. 15 and 16.

The heat flow equation can be solved by the finite element method, a technique that reduces differential equations to a system of algebraic equations [26]. The matrix equations are:

$$\underline{K}\,\underline{T} + \underline{Q} = \underline{C}\,\dot{\underline{T}} \tag{10}$$

where

$\underline{C}$ - heat capacity matrix

$\underline{K}$ - conductivity matrix

$\underline{Q}$ - external heat flow vector

$\underline{T}$ - temperature vector

$\dot{\underline{T}}$ - temperature rate of change vector

Boundary conditions are an integral part of the heat flow equation and represent the effect of external environment on cooling or heating of a structure's surface. These boundary conditions are of two types: (1) temperature (T) specified on the surface, or (2) heat flow (Q) specified across the surface. The first type is useful in modeling thermal loading due to ambient atmospheric changes. As discussed earlier, a modified air temperature (Fig. 5) may be used as the boundary condition for normal environmental exposure. The second type of boundary condition is useful for modeling thermal loading due to fire. The interface between a structure and fire is modeled by an expression defining heat flow across the surface. These boundary conditions account for spatial distribution of fire intensities as well as for convective and radiative heat transfer mechanisms. The heat flux q (heat flow per unit area of exposed surface) may be modeled by a simplified expression commonly used in heat transfer problems as follows:

$$q = A(T_f - T_s)^N + V\sigma\bar{\varepsilon}[\theta_f^4 - \theta_s^4] \qquad (11)$$

where A and N are convection coefficient and power factor, respectively, and T_f and T_s are fire and surface temperatures (both variable in time), V is radiation view factor, σ is the Stefan-Boltzmann constant, $\bar{\varepsilon}$ is an

effective emissivity, and θ_f and θ_s are absolute temperatures of the fire and surface. Specified temperature distribution on the boundary is not generally used for fire exposures, since such distribution is known only when determined experimentally, and therefore is not usually available.

Internal heat generation (term Q in the heat balance equation) can result from an exothermic process such as hydration of cement. Heat release from hydration of cement paste is significant only during the first few weeks after a concrete is mixed. Experimental data indicate great variation among different concretes in the rate of heat release, but much smaller variation in the total amount of heat liberated per unit weight of cement. The following expression has been developed on the basis of these data:

$$H(t)_{current} = H_{total}(1 - e^{-\beta t}) \qquad (12)$$

where

$H(t)_{current}$ - amount of heat liberated per unit weight of cement to time t

H_{total} - total amount of heat liberated per unit weight of cement when hydration is complete (about 28 days)

β - rate constant

t - time in hours

Values of parameter β range from about 0.02 to as low as 0.005. The constant H_{total} is of the order of 100 cal./gm. (18 BTU/lb.) of cement. The actual amount of heat released per cubic foot of concrete is based on cement content in the mix. Heat of hydration is entered in the vector $\underline{Q}$ of the heat balance equation by calculating the time derivative of $H(t)_{current}$.

Use of this model is demonstrated in case studies 2 and 3.

Solution of the matrix heat balance equations is effected by step-by-step time integration; when material properties are temperature dependent as shown in Figs. 15 and 16, a nonlinear iterative technique within each time step is used. The numerical methods for thermal response analysis and the computer program FIRES-T that implements the above models for two-dimensional heat flow are described elsewhere [28]. Once the temperature history of a structure has been determined, associated free volume expansion or contraction is found directly using the coefficients of thermal expansion of the materials involved.

Free Shrinkage Volume Changes

Free shrinkage is the contraction that an element of concrete would undergo if there were no constraint on its movement; hence, free shrinkage differs from apparent shrinkage, the actual measurable movement within a specimen which incorporates both shrinkage and stress-related strains. The development of free shrinkage with time is a complex process, and many mathematical models have been postulated. The model described in this paper, originally suggested by Carlson [29], assumes that moisture content and shrinkage strain are directly related, and that moisture flow within concrete obeys the moisture diffusion equation. However, the mathematical equations and material models will be formulated in terms of shrinkage rather than moisture content [30,31].

$$K_S \left\{ \frac{\partial^2 S(x,y,t)}{\partial x^2} + \frac{\partial^2 S(x,y,t)}{\partial y^2} \right\} + Q_S(x,y,t) = \frac{\partial S(x,y,t)}{\partial t} \qquad (13)$$

The unknown variable $S(x,y,t)$ is shrinkage strain, the specified quantity $Q_S(x,y,t)$ is external shrinkage flow into the section, and K_S is a material parameter. The equation states that shrinkage in an element of concrete must equal shrinkage flow into that element, both from adjacent elements and, if an element is on the boundary, from external sources. For all interior elements, $Q_S = 0$. Note that shrinkage flow is in the opposite direction from moisture flow.

Boundary conditions describe the drying behavior of a concrete surface and only one boundary condition may be specified at each point on a boundary. Different portions of a boundary may have different types of boundary conditions. There are three physically useful types of boundary conditions:

(1) S - shrinkage specified on the boundary

(2) $\frac{\partial S}{\partial n}$ - shrinkage gradient specified on the boundary

(3) Q_S - shrinkage flow specified on the boundary; for a moisture-insulated surface, $Q_S = 0$. A special case is

$$Q_S = f(S_\infty - S)$$

A special case of the second boundary condition is

$$\frac{\partial S}{\partial n} = \frac{f}{K}(S_\infty - S) \qquad (14)$$

The gradient defined by Eq. 14 is such that as surface shrinkage approaches its final value, the gradient will diminish. This seems to model best the drying behavior of concrete and is the boundary condition used in the case studies described in this paper. In this expression, S_∞ is ultimate free shrinkage strain, i.e., the amount of shrinkage that an element of concrete would undergo if it were allowed to dry completely and if there

were no constraint on its movement by adjacent elements. Ultimate shrinkage is very sensitive to the relative humidity of the surrounding environment and to concrete mix materials and composition. Appropriate values of S_∞ must be selected for specific concrete mixes based on experimental data for the given or a similar concrete mix.

The moisture-related properties of concrete are characterized by the following parameters used in the diffusion equation (Eq. 13) and in boundary conditions.

Shrinkage diffusivity -- Diffusivity K_S (in units of $in.^2/day$) models the ease with which shrinkage flows through concrete and is primarily related to moisture diffusivity. Shrinkage diffusivity can be defined as the speed at which shrinkage flows through a material when there exists a unit shrinkage gradient. Previous investigators [31,32] defined diffusivity as time dependent; in this paper, however, diffusivity is assumed to be shrinkage dependent, since this seems to describe best the decline in diffusivity as drying proceeds. Typical values of K_S for concretes are shown in Fig. 17. The effect of temperature on shrinkage diffusivity is neglected.

Surface factor -- Surface factor f (in units of in./day) characterizes the speed of surface evaporation and controls the shrinkage boundary condition at drying surfaces. Hence, strictly speaking, f can be a surface property as well as a material property. This material parameter can have its own functional form and be independent of other material parameters; for ease of calculation, however, it is most commonly assumed that f is directly proportional to K_S. In this paper, the following relation (similar to Pickett's) is used:

$$f(S) = 1.67K(S) \tag{15}$$

Finite elements can be used to reduce the shrinkage balance equation to matrix form:

$$\underline{K}\,\underline{S} + \underline{Q} = \underline{V}\,\dot{\underline{S}} \tag{16}$$

where

$\underline{K}$ - shrinkage diffusivity matrix

$\underline{V}$ - shrinkage velocity matrix

$\underline{Q}$ - external shrinkage flow loading vector

$\underline{S}$ - nodal shrinkages

$\dot{\underline{S}}$ - nodal shrinkage velocities

This matrix equation is solved in essentially the same manner as the heat balance equation. Numerical techniques as well as a description of a computer program (SHRINC) implementing the model developed herein are described elsewhere [32].

STRUCTURAL ANALYSIS

Once all modeling assumptions have been made, it is possible to proceed with the structural analysis. A modification of the direct stiffness method of matrix structural theory is used: the frame is discretized into beams and columns (members) and the stiffness matrix of each member is assembled into an overall structural stiffness matrix. This defines the equilibrium equations at each joint of the frame.

$$[K(u,t)]\,\{u\} = \{P\} \tag{17}$$

where $[K(u,t)]$ is the time- and deformation-dependent structural stiffness matrix, $\{u\}$ is the joint deformation matrix, and $\{P\}$ is the joint loading matrix. Because the nonlinearity of material behavior causes the

stiffness matrix to change with time and deformation, the equilibrium equations are nonlinear and Eq. 17 must be solved iteratively using a Newton-Raphsen technique.

The stiffness matrix of each member is derived by considering the state of stress and degradation in each concrete or steel element to derive an averaged segment stiffness, which in turn is combined with other segment stiffnesses to form an overall member stiffness. When assembled, these member stiffnesses constitute the frame tangent stiffness for the environmental and stress conditions existing at that particular instant.

Detailed explanation of the above structural analysis techniques and of computer programs implementing them can be found in References 34 through 39.

CASE STUDIES

The methods described above were applied to four case studies; results are presented and briefly discussed below. In the first two studies, analytical results were correlated with experimental results from studies on shrinkage in specimens of varying size. In the third study, the method was applied to a special problem in concrete construction under permafrost conditions. In the fourth and final study, the response of reinforced concrete frame elements to a hypothetical compartment fire was analyzed.

Case Study 1

An extensive series of tests on concrete shrinkage of two sizes of cylindrical specimen was carried out by J. Keeton [40]. Three-inch diameter by 9-inch long, and 6-inch diameter by 18-inch long cylindrical specimens were allowed to dry for periods of several years in a carefully controlled 50% R.H. and 68°F environment.

Available data on the properties of concrete used in this series of tests are incomplete. Only compressive strength and modulus of elasticity at 28 days were reported. No data were available on creep, tensile strength, effects of aging on mechanical properties, or thermal properties of the concrete. Creep and tensile strength for this concrete were estimated for this study, but thermal and aging effects were neglected. Shrinkage diffusivity K_S and ultimate shrinkage S_∞ were estimated from data on the smaller specimens and appeared to be relatively high. Values of K_S for this concrete (designated A) are shown in Fig. 17. Other material properties are given in Table 2.

Drying of these two types of specimens was simulated using the two-dimensional analytical methods developed in this paper. Effects of heat of hydration were neglected in this analysis. Cross sections for both cylinders were discretized using 100 elements per quadrant as shown in Fig. 18. A drying boundary condition of the second type (Eq. 14) was used. Time steps were varied throughout the drying period, starting with 1-day steps and increasing gradually to 100-day steps after about 300 days of drying.

Free shrinkage gradients, compressive stresses in the interior, and tension stresses and cracking in exterior elements will be reported elsewhere. In this paper, only comparisons of experimental and analytical data for apparent shrinkage strains of the 3- and 6-inch specimens are shown in Fig. 19. The excellent correlation between analytical and experimental results suggests that the proposed analytical methods based on size-independent diffusivity and ultimate shrinkage can adequately predict apparent shrinkage in specimens of varying size.

Mechanical properties of the 3- and 6-inch diameter cylinders were

assumed to be identical. Actually, different dissipation rates of heat of hydration result in differences in curing temperature in portions of specimens of different size, in mechanical properties, and in effects of aging on these properties in the two specimens. Some discrepancies between analytical and experimental results may be explained by the preceding factors having been neglected in the analysis. To explore these differences, further comparisons of analytical and experimental data for larger specimens were made; results are presented in the second case study.

Case Study 2

A series of tests to explore the effect of specimen size on apparent shrinkage was carried out by Mamillan [41]. Square prismatic specimens ranging in size from 8.25 to 39.3 inches were made from the same concrete and left to dry at 55% R.H. and 68°F for periods of up to 3 years. Data on concrete properties available to the authors were incomplete. Most thermal and mechanical properties assumed for this concrete (designated B) were therefore best estimates.

Temperature variations due to heat of hydration can be expected to result in volume changes that could significantly affect induced stresses and final deformation for larger specimens. To verify this hypothesis, a thermal analysis of the effect of heat of hydration was carried out for all sizes of specimens. Two simplifying assumptions were made: (1) shrinkage diffusion coefficients and ultimate shrinkage values were assumed to be temperature independent, and (2) mechanical properties were assumed to be nonaging and temperature independent.

In the first analysis of this case study, free shrinkage and stress-related deformation were considered, while thermal deformation was not.

In the second analysis, thermal deformation as well as free shrinkage and stress-related deformation were accounted for. Square prismatic cross sections were discretized using 100 elements per quadrant as shown in Fig. 18; the drying boundary conditions defined by Eq. 14 were used. Time steps for the thermal analysis were smaller, starting with 1-hour increments and increasing gradually to 1-day increments during the first month. For shrinkage and stress analysis, time steps similar to those used in the first case study were used.

The calculated temperature history at the center of each prism is shown in Fig. 20. For the 39.3-inch prism, the temperature rose about 17°F during the first days and then returned to approximately the original value within 30 days. For smaller specimens, temperature rise was negligible.

Comparisons of calculated apparent shrinkage strain with measured values for specimens of different size are shown in Fig. 21. Agreement was quite good for the 8.25-inch and 16.5-inch prisms in which the effects of thermal deformation were negligible. For the largest prism (39.3 inches), strains observed during the first few days were primarily due to thermal effects and were in good agreement with predicted values. After this period, the analysis indicated a much faster rate of apparent shrinkage than that measured in the 39.3-inch specimens. This overestimation was probably due to the assumption that aging does not affect elastic and creep properties. At early ages, the lower stiffness of concrete leads to a slower rate of stress-related deformation.

No definitive conclusions can be derived from these two studies because the good agreement for cylinders and prisms up to 16 inches in size was contrasted by poor agreement for the 39.3-inch prisms. The discrepancy was probably due to inadequate modeling of early age properties

and subsequent aging effects on these properties which have a greater influence on larger specimens. Experimental data not presently available would be needed to develop such models.

Case Study 3

A case study based on a problem that arose during construction of pier foundations for a pipeline and vehicular bridge across Alaska's Sagavarnirktok River was carried out.* The piers were 36-inch diameter steel pipes grouted within a 45-inch diameter hole drilled in permafrost. The grout placed in the annular space between the pier and the permafrost was required to attain a minimum strength within a specified time. To attain this strength, it was necessary to maintain the temperature of the grout above freezing for a period of time to ensure adequate curing. Because the ambient air temperature was estimated at -40°F, and because the permafrost temperature was estimated at 20°F, the problem of maintaining the grout at temperatures above 32°F required that an adequate source of heat input be provided. In this study, the problem was to determine temperature distribution and history in the grout when the interior of the steel pipe pier is filled with concrete mixed with Type III cement. The idealized geometry of the pier and a sector from a transverse section are shown in Fig. 22.

It was assumed that no heat flowed along the longitudinal axis of the pile; hence, the thermal analysis reduced to a two-dimensional heat flow problem. It was also assumed that heat flow was axisymmetric so that the

---

*The general information defining this problem was provided through the courtesy of Earl & Wright, Civil Engineers, S.F., California, and Ben C. Gerwick, Jr., Consulting Engineer, S.F., California.

geometric model shown in Fig. 22 was suitable for the analysis. Boundary conditions were modeled assuming a fixed temperature of 20°F at a radius of 36 inches (Fig. 22), since it was assumed that the temperature of the permafrost would be undisturbed at that distance from the concrete fill.

Total heat generation, H_{total}, was estimated to be 100 cal./gm. (18 BTU/lb.) of cement. The grout contained 30% and the concrete 13.5% cement by weight, resulting in total heat generation values of 8100 BTU/ft.^{3} and 3600 BTU/ft.^{3}, respectively. The rate of heat release was calculated using the exponential expression for H (heat released):

$$H_{released} = H_{total}(1 - e^{-\beta t})$$

Two rate parameters, $\beta = 0.0167$ and $\beta = 0.0083$, were considered in the analyses. Thermal properties of the various materials are shown in Table 3.

A layer of permafrost adjacent to the grout was above 32°F, so that the ground was not frozen but waterlogged. The thickness of this layer is not known and probably varied with time. In this analysis, the layer was assumed to have a constant thickness of 1 inch. This assumption is important because the water layer acted as a sort of insulation to heat dissipation. The thermal properties of the permafrost and of the waterlogged layer were somewhat difficult to estimate. For this analysis, thermal properties of the permafrost were assumed to be the same as those of the concrete. For the waterlogged layer, K was taken as 0.33 BTU/(ft. x hr. x °F) while C and ρ were assumed to be identical to those for the concrete.

It was further assumed that the concrete and grout were mixed with hot water and had an initial temperature of 40°F, that the pipe had an

initial temperature of -20°F, and that the time lag between placement of concrete and grout was small and negligibly affected temperature history. The wedge was discretized by 29 finite elements. Forty time steps of 5 hours each were used.

Thermal results are shown in Fig. 23 and in Table 4. Note that grout temperatures at the outer edge of the caisson were calculated for 3 possible conditions: (A) normal heat release (β = 0.0167) and conductivity (K = 1.5 BTU/(ft. x hr. x °F), (B) heat release as in (A) but lower conductivity of 1.0 BTU/(ft. x hr. x °F), (C) a lower rate of heat release (β = 0.0083) and conductivity as in (A). It can be seen that while the maximum temperature attained by the grout at the outer edge was sensitive to such parameters as heat release and conductivity, the time to freezing and maximum temperature were relatively less sensitive to these parameters.

Temperature distribution within the foundation pier for the first case is shown in Fig. 24. The average grout temperature was several degrees higher (2°F - 5°F) than the outer edge temperature. Based on results of this analysis (Figs. 23 and 24) it was estimated that the grout remained at a temperature above freezing for a period of approximately 7 days.

Case Study 4

Thermal and structural response of reinforced concrete frames to fire have been investigated analytically using the method outlined in this paper [35,42,43]. The following example illustrates the general procedure; the more important results of the study are discussed below.

Figure 25 shows the plan and section of the 13-story reinforced concrete frame analyzed for thermal and structural response to fire. A fire was considered to have occurred on the 12th story of the building involving two 32-foot bay compartments. Two types of fire action -- a

long duration, moderate intensity fire (ASTM E-119), and a short duration, high intensity fire (SDHI) -- were considered. The time-temperature curves for these two fires are shown in Fig. 26.

In order to reduce computational effort, the multistory building was modeled by an isolated substructure as shown in Fig. 25. The substructure included one story above and one below the fire level. The columns of the 11th story were assumed to be fully restrained at the base, leading to the 3-story model shown in Fig. 25. It was assumed that the dead weight of the structure plus 60% of the design live load were acting during the fire process. All loads were assumed to be uniformly distributed over the floors of the building, and the loads acting on the beams were calculated on the basis of contributary floor areas bounded by mid-bay and 45° lines.

The characteristics of the column and floor beam cross sections in the 3-story substructure were as follows. Columns were 20 inches square with 8 No. 7 bars (steel ratio $\rho = 0.013$). All beams were T-shaped with a 6-inch thick and 34-inch wide flange, a 10-inch wide stem, and an overall depth of 18.5 inches. T-beam bottom steel reinforcement consisted of 3 No. 6 bars ($\rho_s = 0.007$) and top reinforcement consisted of 3 No. 6 bars and 8 No. 5 bars ($\rho_s' = 0.02$). The No. 5 bars also served as bottom slab reinforcement. At normal temperatures, the concrete design compressive strength f_c' was 5050 psi, and the steel yield strength f_y was 60,000 psi. Thermal and mechanical properties and their variation with temperature generally conformed to models outlined in this paper.

Typical results of the thermal analysis from computer program FIRES-T are shown in Figs. 27 and 28. The temperature distribution in the 3 members surrounding the fire compartment are shown after the ASTM fire had acted for 0.5 hour. The isotherms for the SDHI fire for 0.5-hour

duration are quite similar, but by the surface of the cross section were much lower. However, for the ASTM case, temperatures continued to rise, the maximum concrete temperature in the column approaching 1600°F and the maximum reinforcing steel temperature (corner bar) reaching 800°F. For the SDHI fire, temperatures rose little after 0.5 hour. In the column, maximum concrete temperature barely exceeded 600°F and maximum reinforcing steel temperature reached only 400°F. It is important to note that the presence of reinforcing steel influenced the temperature as reflected in the shape of the isotherms.

Structural behavior is illustrated in Figs. 29 and 30 where the deformation of the frame model due to each fire is shown. This analysis was conducted using computer program FIRES-RC II. The first 0.5 hour of each fire led to large thermal expansion in the floor beams above and below the fire compartment, pushing the girders in adjacent bays outward and causing large internal translation of the columns in the fire story. Lateral displacement of joints at this level was restrained by beam and column frame elements away from the fire zone. Thus, significant compression forces developed in the floor girders just above and below the fire. The girders further removed from the fire level (roof girders) acted as ties restraining lateral displacement at the fire level, and significant tension forces developed. The base of the 3-story model also resisted lateral displacement of the heated girders, so that the actual 13-story frame could be expected to exhibit high tension in floor beams at this level, and at several lower levels although to a lesser extent. In addition, the large lateral displacements forced upon the columns adjacent to the fire level (11th and 13th stories) generated significant shear forces and bending moments in these elements. Thermal expansion of the column of the fire story was relatively small compared to that of the

girders because of the column's greater size; hence, vertical displacements due to the fire were of much less importance than lateral expansion.

The girders directly above and below the fire developed large moments due to restraints imposed on thermally induced curvatures. These members suffered severe degradation of cross-sectional stiffness, as illustrated in Fig. 31 for the ASTM fire of 0.5-hour duration. The pattern for the SDHI fire is very similar at this time. The concrete directly exposed to fire developed large compression stresses due to thermal gradients and crushed early. In modeling the structural behavior of concrete in FIRES-RC II, it is assumed that a state of 'crushing' corresponds to a large compression strain in concrete, ε_u, at which concrete can no longer sustain any significant compression. In this study, a constant value of 0.004 was assumed for ε_u. The concrete on the cool side of the T-beam cracked due to large restraining end moments opposing the end rotations which would result from thermal gradients in a free condition. Cracking was assumed to occur when the tensile strength of concrete was exceeded (590 psi at 0°F, decreasing linearly to 120 psi at 1200°F; constant 120 psi for temperatures greater than 1200°F).

The fire-exposed column behaved in much the same way, but degraded less due to greater stiffness and lower average temperature. Cracking and crushing patterns are shown for the ASTM fire of 0.5-hour duration in Fig. 32.

It is interesting to note that bending moments in members in regions outside the fire compartment increased greatly due to the action of the fire during the first 0.5 hour of exposure. End moments in girders not exposed to the fire increased by a factor of 2 to 4, and in columns by 2 or 3 orders of magnitude. Such increases result in cross-sectional

degradation which was often considerable at these points due to increased cracking.

For the final 0.5 hour of analysis, behavior differed quite markedly from that described above for the first 0.5 hour. In the SDHI fire, temperatures dropped and the frame suffered no additional degradation, surviving the fire without collapse. However, in the ASTM fire, temperatures within heated members continued to increase, girders above and below the fire underwent even greater degradation (cracking and crushing), and deformations became quite large (Fig. 29). Finally, just before 0.75 hour, the floor girder of the fire compartment failed in flexure, losing all stiffness. At this point, the FIRES-RC II analysis terminated.

The results presented above clearly demonstrate the importance of frame distortion and cross-sectional degradation (cracking and crushing) in evaluating the redistribution of forces and moments, and the resistance capacity of the system. In particular, large increases in column shear and moment can cause local failures and, in the case of long duration fires, may lead to progressive collapse. Tension forces in girders that develop in zones not involved but adjacent to a fire can also reduce the capacity of girders to resist shear and increased moment due to fire. Also, possible reversal in moment in some regions of girders could lead to failure during cooling phases of a fire. Improvements in fire safety may call for special detailing requirements while an increase in size or in steel reinforcement may not necessarily improve structural response.

The results also clearly demonstrate that fire tests on isolated structural elements such as columns, girders, and floor panels cannot fully account for the behavior of elements in place. Development of improved designs for fire resistant structures therefore requires a

coordinated approach, using both analytical and experimental methods.

CONCLUSIONS

The complex nature of environmental and loading conditions that occur during the lifetime of a structure is no longer beyond practical solution. In this paper, several models that can aid in obtaining such solutions were described. In particular, ambient temperature variations and fire exposure models can be useful in developing better practical design criteria for reinforced concrete frame structures.

In order to obtain reliable predictions of structural response, the essential features of nonlinear, time-dependent, and nonhomogeneous material behavior must be accounted for properly. For concrete, heat of hydration, nonhomogeneous temperature distribution and drying, as well as changing properties during early ages, may be important in predicting long-time effects, particularly cracking and deformation.

In this paper, several case studies were included where agreement between calculated and observed shrinkage was very good. In cases where comparison of experimental and analytical results was less satisfactory, discrepancies can be attributed to inadequate understandings of concrete behavior at early ages. While no specific verification of predicted temperatures in the pier of the Sagavarnirktok River Bridge is available, the predicted overall maturity of the grout appears to have been verified. The behavior of the frame exposed to fire [43] presented in this paper definitely points to the need for better design of certain columns and connections in reinforced concrete frames exposed to certain types of fire. The relatively good record of building performance in fires may be more the result of the efficiency of fire service measures than of the reliability of structural design for extreme exposures.

The overview of the methodology and the results presented here point out a number of areas where more information is needed to predict structural response yet more reliably. The more important among these are experimental studies of plain concrete and reinforcing steel properties under combined variable environment (temperature, humidity) with variable stress history (short-term cycling as well as long-term sustained and variable loads). Analytical methods and environmental models can be useful in constructing better models of material behavior. To verify and improve the analytical models proposed here, it will also be necessary to study reinforced concrete frames experimentally.

For special structures and for extremely complex environments, the analytical methods described here can be used to verify the adequacy of required performance directly. However, the ultimate objective of this work is to aid in developing simple practical design criteria.

ACKNOWLEDGMENTS

The continuing support of the National Science Foundation through its RANN Program (Research Applied to National Needs) is gratefully acknowledged.

Special thanks are due to Ben C. Gerwick, Jr., Consulting Engineer, and Earl & Wright, Civil Engineers, both of San Francisco, California, for providing data on the Sagavarnirktok River Bridge problem.

The authors also wish to express their appreciation to Z. Nizamuddin and G. Thielen for their help in developing Case Study 4. The assistance of J. Sanders in editing the manuscript and of G. Feazell and L. Rambeau in preparing the graphics is gratefully acknowledged.

REFERENCES

1. Robertson, L. E. and Chen, P. W., "Effects of Environmental Loads on Tall Buildings," Proceedings of the U.S.-Japan Seminar on Wind Loads on Structures, University of Hawaii, Hawaii, October 1970.

2. Dempsey, B. J. and Thompson, M. R., "A Heat Transfer Model for Evaluating Frost Action and Temperature Related Effects in Multilayered Pavement Systems," Civil Engineering Studies, Highway Engineering Studies No. 41, University of Illinois, Urbana, June 1971 (also published in Highway Research Record 342, 1970).

3. Mackey, C. O. and Wright, J. H., "Summer Comfort Factors as Influenced by the Thermal Properties of Building Materials," Transactions of the American Society of Heating and Ventilating Engineers, 1942.

4. Sahota, M., "Heat and Mass Transfer in Porous Concrete Structures Subject to Fire," Report No. UCB FRG 76-15, Fire Research Group, Division of Structural Engineering and Structural Mechanics, Department of Civil Engineering, University of California, Berkeley, September 1976.

5. Harmathy, T. Z., "A New Look at Compartment Fires - Parts I and II," Fire Technology, August and November 1972, pp. 197-217 and pp. 327-351.

6. Law, M. and Arnault, P., "Fire Loads, Natural Fires and Standard Fires," ASCE-IABSE International Conference on Planning and Design of Tall Buildings, Lehigh University, Bethlehem, Pennsylvania, August 21-26, 1972, Conference Preprints: Reports Volume 1b-8, pp. 13-28.

7. Magnusson, S. E. and Thelandersson, S., "Temperature-Time Curves of Complete Fire Process of Fire Development," Civil Engineering and Building Construction Series No. 65, Division of Structural Engineering and Concrete Construction, Lund Institute of Technology, Lund, Sweden, 1970.

8. Robertson, A. F. and Gross, D., "Fire Load, Fire Severity, and Fire Endurance," ASTM STP 464, 1970, pp. 186-208.

9. Aleksandrovski, S. V., Design of Concrete and Reinforced Concrete Structures for Variable Temperature and Humidity Including Effects of Creep, Second Edition, Stroiisdat, Moscow, U.S.S.R., 1973 (in Russian).

10. Bazant, Z., "Creep and Shrinkage of Concrete: A Precis of Recent Developments," Mechanics Today, Vol. 2, 1974, pp. 1-93.

11. Bazant, Z. P. and Najjar, L. J., "Drying of Concrete as a Nonlinear Diffusion Problem," Cement and Concrete, Vol. 1, 1971, pp. 461-473.

12. Bazant, Z. P. and Najjar, L. J., "Nonlinear Water Diffusion in Nonsaturated Concrete," RILEM Materiaux et Construction, Vol. 5, No. 25, January-February 1972.

13. Powers, T. C., "Mechanisms of Shrinkage and Reversible Creep of Hardened Cement Paste," Proceedings of an International Conference on the Structure of Concrete and its Behavior under Load, Cement and Concrete Association, London, 1968.

14. Considere, A., Experimental Researches on Reinforced Concrete, translated by Leon S. Moiseiff, McGraw Hill Publishing Company, New York, 1903.

15. Mikhailov, V. V., "Extensibility of Concrete under Conditions of Free and Restrained Deformation," Proceedings of the Conference on Theory of Technology, Armenian Academy of Sciences, A.S.S.R., Erevan, 1956 (in Russian).

16. Scanlon, A., "Time-Dependent Deflections of Reinforced Concrete Slabs," Ph.D. Dissertation, Department of Civil Engineering, University of Alberta, Edmonton, Canada, December 1971.

17. Anderberg, Y. and Thelandersson, S., "A Constitutive Law for Concrete at Transient High Temperature Conditions," Douglas McHenry Symposium Volume, American Concrete Institute, Detroit, Michigan, 1977.

18. Furumura, F., "The Stress-Strain Curve of Concrete at High Temperatures," Report of Meeting of the Architectural Institute of Japan, Tokyo Institute of Technology, 1966.

19. Pister, K. S., Argyris, J. H., and William, K. J., "Creep and Shrinkage of Aging Concrete," Douglas McHenry Symposium Volume, American Concrete Institute, Detroit, Michigan, 1977.

20. Mukaddam, M., "Behavior of Concrete under Variable Temperature and Loading," Final Report, IABSE Symposium: Design of Concrete Structures for Creep, Shrinkage and Temperature Changes, Madrid, 1970, pp. 301-310.

21. Mukaddam, M., "Creep Analysis of Concrete at Elevated Temperatures," Journal of the American Concrete Institute, Vol. 71, February 1974, pp. 72-79.

22. Mukaddam, M. A. and Bresler, B., "Behavior of Concrete under Variable Elevated Temperature and Loading," American Concrete Institute STP 34, Paper No. 37, 1972, pp. 771-797.

23. Sackman, J. L., "Creep of Concrete and Concrete Structures," Proceedings of the Princeton University Conference on Solid Mechanics, Princeton University, Princeton, New Jersey, 1965, pp. 15-48.

24. Sherby, O. and Dorn, J. E., "An Analysis of High Temperature Creep," Proceedings of the Society for Experimental Stress Analysis, Vol. 12, 1953, p. 139.

25. Harmathy, T. Z. and Stanzak, W. W., "Elevated Temperature Tensile and Creep Properties of Some Structural and Prestressing Steel," American Society for Testing and Materials STP 464, 1970, pp. 186-208.

26. Zienkiewicz, O. C., The Finite Element Method in Engineering Science, McGraw Hill Publishing Company, Berkshire, England, 1971.

27. ACI Committee 207, ACI Manual of Concrete Practice - Part 1, "Mass Concrete for Dams and Other Massive Structures," Detroit, Michigan, 1972, pp. 207-1 to 207-37.

28. Becker, J. M., Bizri, H., and Bresler, B., "FIRES-T - A Computer Program for the FIre REsponse of Structures - Thermal," Report No. UCB FRG 74-1, Fire Research Group, Division of Structural Engineering and Structural Mechanics, Department of Civil Engineering, University of California, Berkeley, 1974.

29. Carlson, R. W., "Drying Shrinkage of Large Concrete Members," Journal of the American Concrete Institute, Vol. 8, No. 3, January-February 1937, pp. 327-336.

30. Bresler, B., Helmich, D., and Ramakrishna, L. V., "Nonuniform Drying Shrinkage in Reinforced Concrete," Preliminary Publication, IABSE Symposium: Design of Concrete Structures for Creep, Shrinkage and Temperature Changes, Madrid, 1970, pp. 171-179.

31. Pickett, G., "Shrinkage Stresses in Concrete," Journal of the American Concrete Institute, Vol. 42, January-February 1946.

32. Polivka, R. and Bresler, B., "Time-Dependent Behavior of Reinforced Concrete Columns Including Effects of Shrinkage, Creep and Cracking," Report No. UC-SESM 75-5, Division of Structural Engineering and Structural Mechanics, University of California, Berkeley, June 1975.

33. Iding, R. H. and Bresler, B., "SHRINC - A Computer Program for Nonuniform Drying Shrinkage in Concrete Members," Report No. UC-SESM 75-8, Division of Structural Engineering and Structural Mechanics, University of California, Berkeley, 1975.

34. Becker, J. M. and Bresler, B., "FIRES-RC - A Computer Program for the FIre REsponse of Structures - Reinforced Concrete Frames," Report No. UCB FRG 74-3, Fire Research Group, Division of Structural Engineering and Structural Mechanics, Department of Civil Engineering, University of California, Berkeley, 1974.

35. Becker, J. M. and Bresler, B., "Reinforced Concrete Frames in Fire Environments," Proceedings of the American Society of Civil Engineers, Vol. 103, No. ST1, January 1977, pp. 211-224.

36. Bizri, H., "Structural Capacity of Reinforced Concrete Columns Subjected to Fire Induced Thermal Gradients," Report No. UC-SESM 73-1, Structural Engineering Laboratory, University of California, Berkeley, 1973.

37. Bresler, B., "Some Factors in the Investigation of Long Term Behavior of Reinforced Concrete Structures," Laboratory Note No. LN/150/BB, Road Research Laboratory, DSIR, England, August 1962.

38. Iding, R., et al., "FIRES-RC II - A Computer Program for the FIre REsponse of Structures - Reinforced Concrete Frames - Second (Revised) Version," Report No. UCB FRG WP 76-7, Fire Research Group, Division of Structural Engineering and Structural Mechanics, Department of Civil Engineering, University of California, Berkeley, 1977 (in preparation).

39. Iding, R. and Bresler, B., "SASHTEC - A Computer Program for Structural Analysis of Shrinkage and Temperature Effects in Reinforced Concrete Frames," Division of Structural Engineering and Structural Mechanics, University of California, Berkeley (in preparation).

40. Keeton, J. R., "Study of Creep in Concrete, Phase I (I-BEAM)," Technical Report R333-1, U.S. Naval Civil Engineering Laboratory, Port Hueneme, California, 1965.

41. Mamillan, M., "Influence de la Dimension des Eprouvettes sur le Retrait," Anales de L'Institute Technique du Batiment et des Travaux Publics, No. 258, Paris, June 1969.

42. Bresler, B., "Response of Reinforced Concrete Frames to Fire," Preliminary Report, 10th Congress of the IABSE, Tokyo, September 6-11, 1976, pp. 273-280.

43. Bresler, B., et al., "Limit State Behavior of Reinforced Concrete Frames in Fire Environments," Proceedings of the Regional Conference on Tall Buildings, Hong Kong, September 20-22, 1976, Institution of Structural Engineers and the Joint Committee on Tall Buildings, 1976.

TABLE 1 RANGES OF CHARACTERISTIC TIMES AND TEMPERATURES

Characteristic times, minutes	$5<t_1<25$	$5<t_2<75$	$10<t_3<100$	$60<t_4<400$
Characteristic temperature rates, °F/min.	$80<\dot{T}_1<200$	$0<\dot{T}_2<5$	$10<\dot{T}_3<50$	--

TABLE 2 CONCRETE CHARACTERISTICS

	Concrete A	Concrete B
Mechanical Properties		
Compressive strength, f_c, psi	7000	5000
Tensile strength, f_t, psi	900	500
Elastic modulus, E_c, psi	3.8×10^6	3.8×10^6
Shrinkage Properties		
K_s	see Fig. 17	see Fig. 17
S_∞	1000×10^{-6}	390×10^{-6}
f	$1.67\ K_s$	$1.67\ K_s$
Thermal Properties		
Coefficient of thermal expansion °F	--	6×10^{-6}
Thermal conductivity (BUT/ft. x hr. x °F)	--	1.00
Heat capacity (BTU/lb. x °F)	--	0.272
Heat of Hydration (BTU/ft.^{3})	--	3600
Coefficient β (index of heat evolution rate)	--	0.005
Physical Properties		
Density (lb./ft.^{3})	--	150

TABLE 3 THERMAL PROPERTIES AND DENSITY

	Steel	Concrete	Grout
Thermal Conductivity K - BTU/(ft. x hr. x °F)	30	1.0-1.5	1.0-1.5
Specific Heat C - BTU/(lb. x °F)	0.11	0.272	0.272
Density ρ - lb./ft.^{3}	489	150	150

TABLE 4 MAXIMUM TEMPERATURE AND TIME TO FREEZING FOR VARYING CONDITIONS

Case	Conductivity	Rate of Heat Release	Max. Temp.		Time Days to Freezing
			°F	Days	
A	normal	normal	48	1.9	6.25
B	low	normal	52	2.3	8.13
C	normal	low	38	2.1	6.7

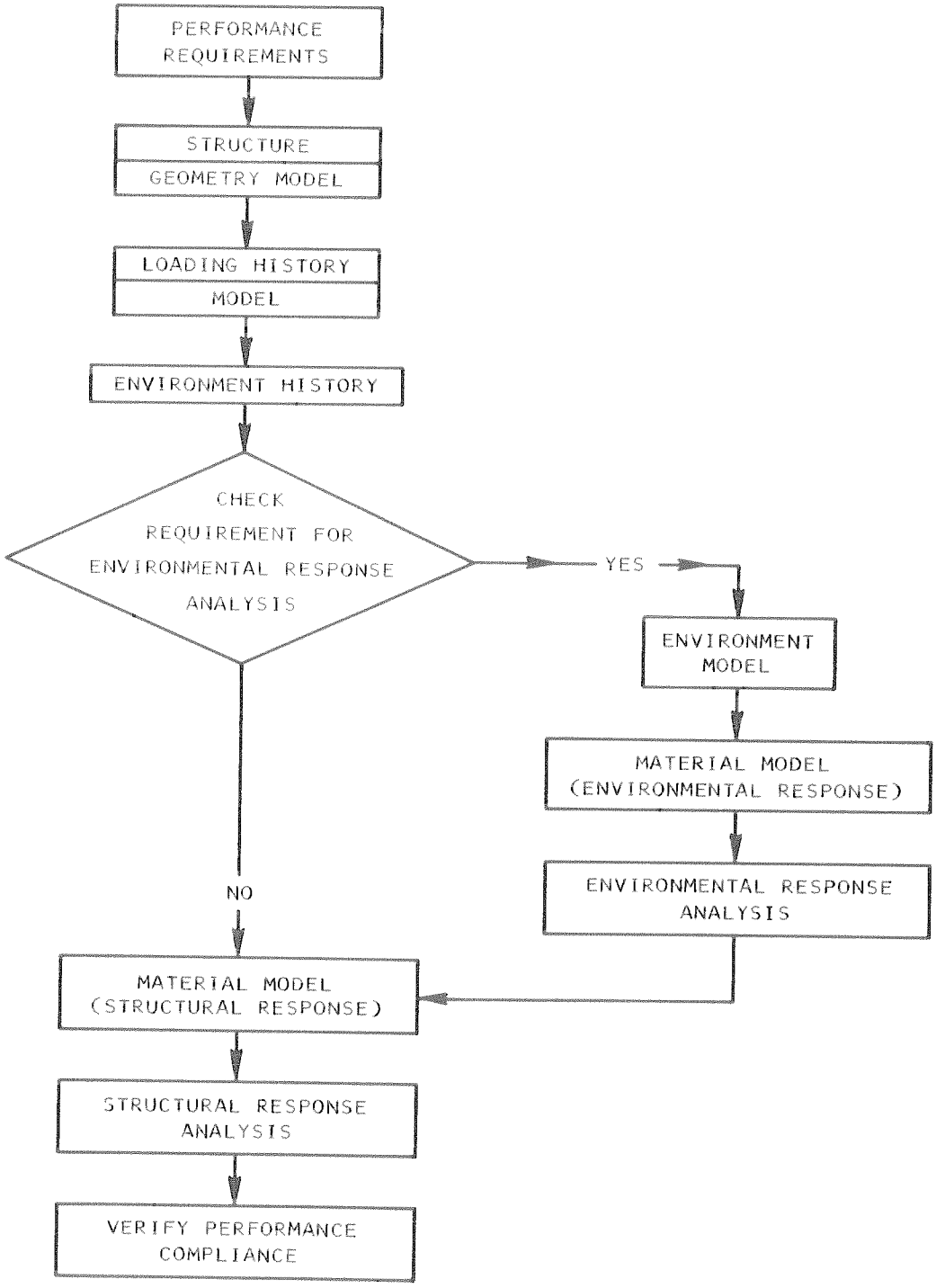

FIGURE 1 DESIGN PROCESS - FLOW CHART

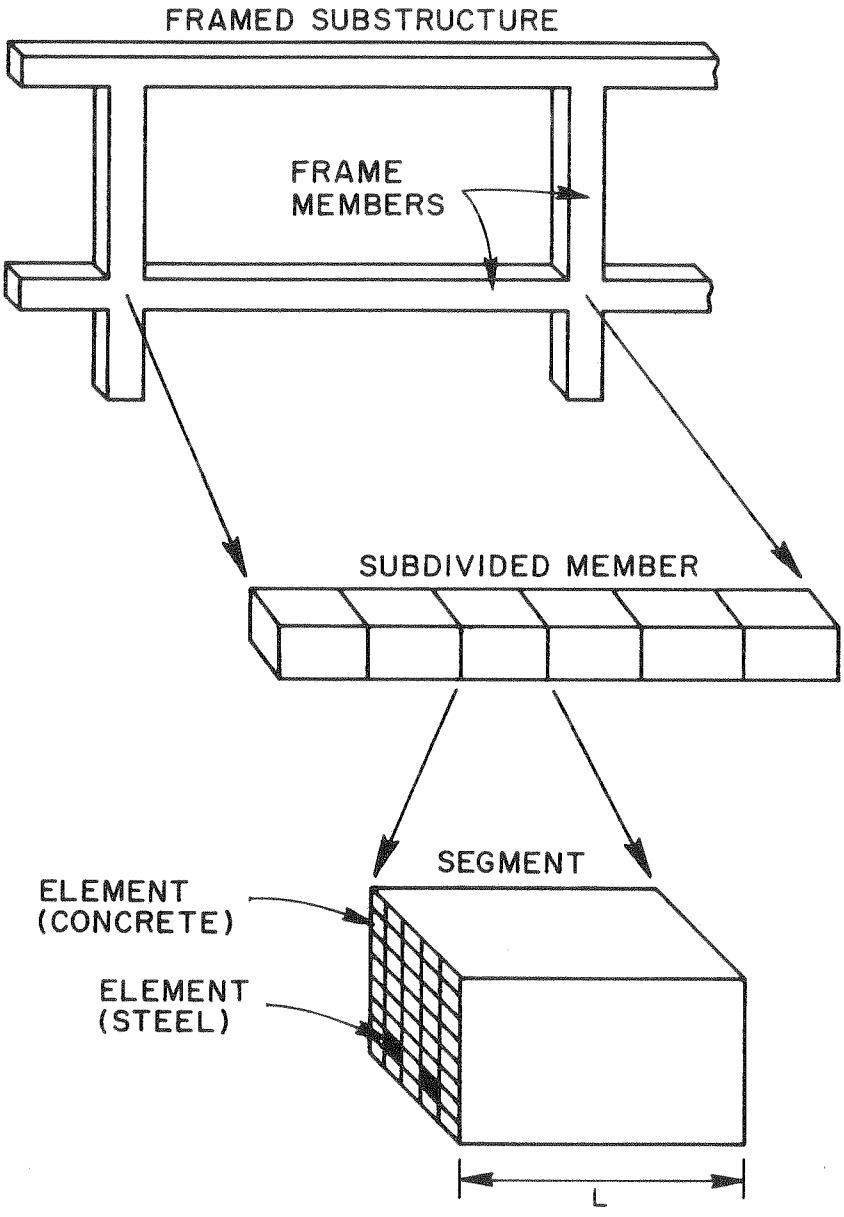

FIGURE 2 GEOMETRIC IDEALIZATION

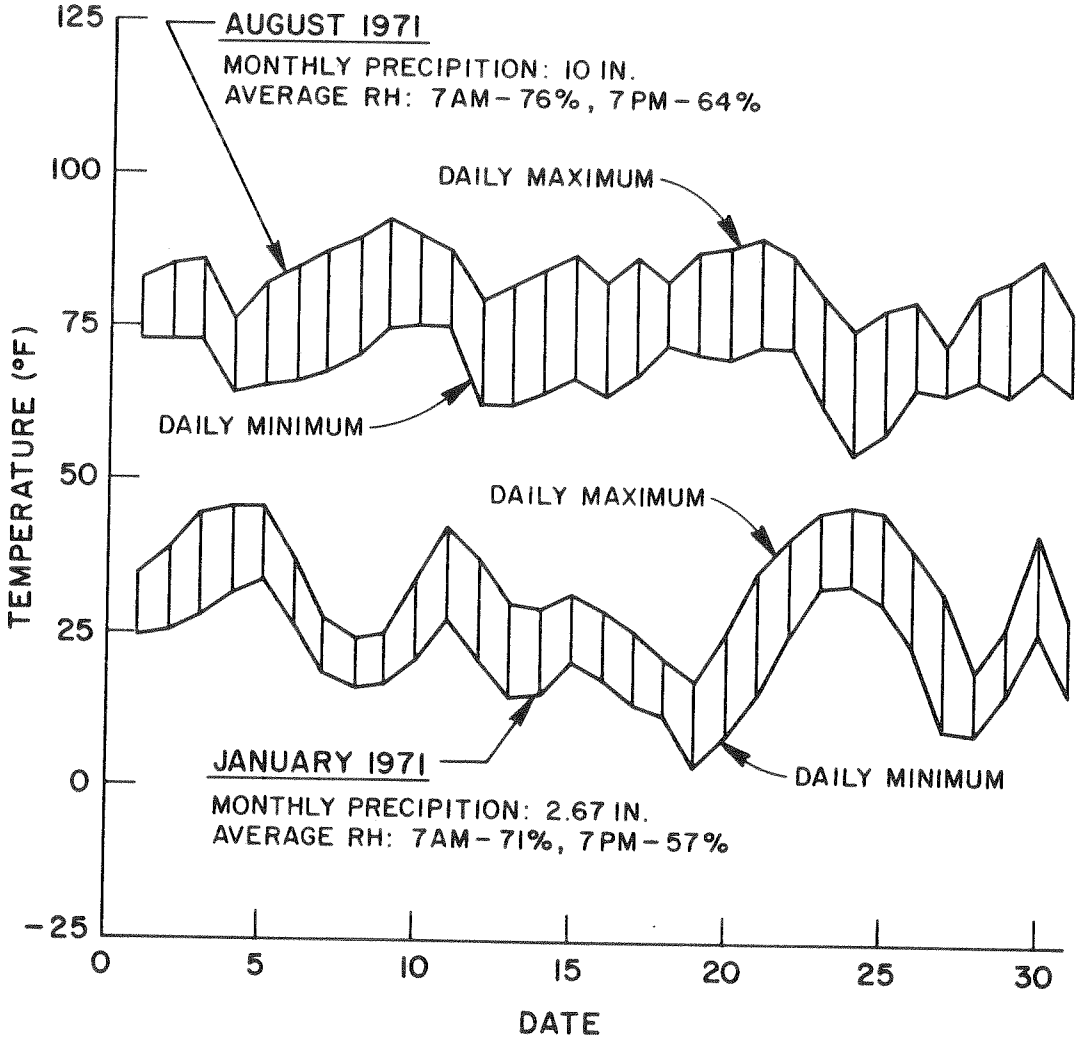

FIGURE 3 TYPICAL VARIATIONS IN DAILY TEMPERATURES FOR NEW YORK (CENTRAL PARK WEATHER STATION)

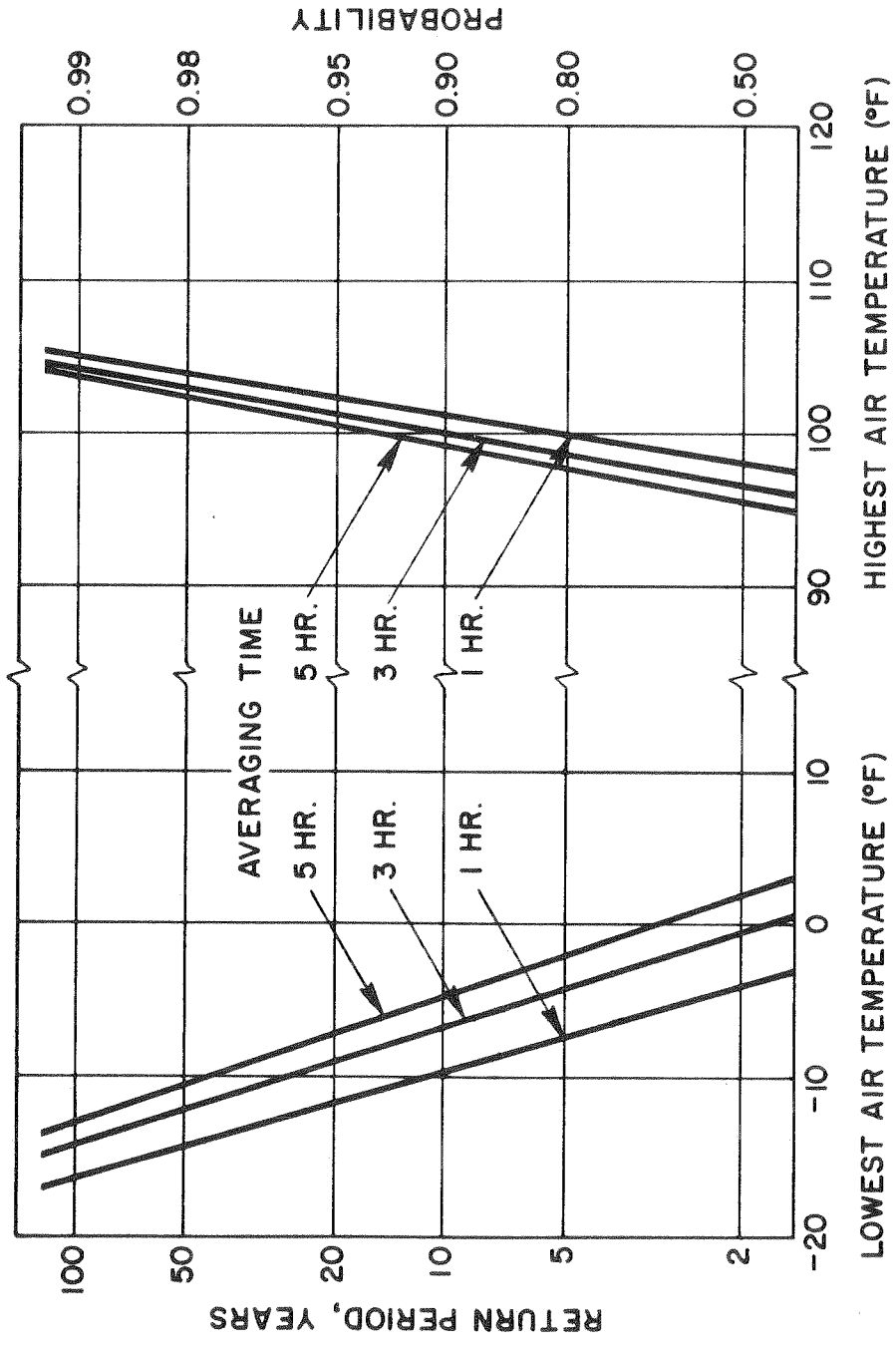

FIGURE 4 EXTREME VALUES - AIR TEMPERATURES (PITTSBURGH, PA. [1])

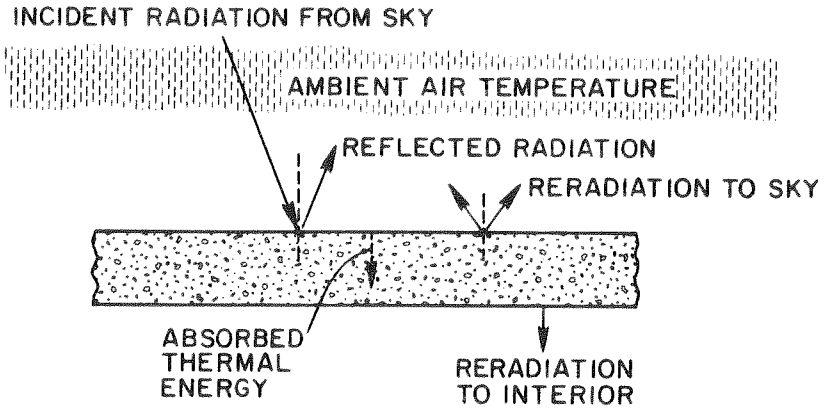

(a) REAL CONDITIONS

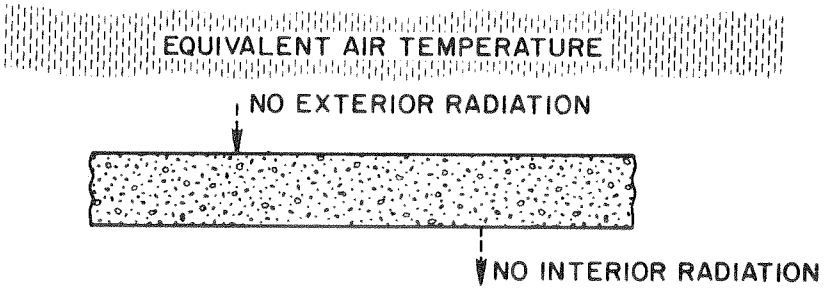

(b) MODEL PROPOSED BY MACKEY AND WRIGHT (3)

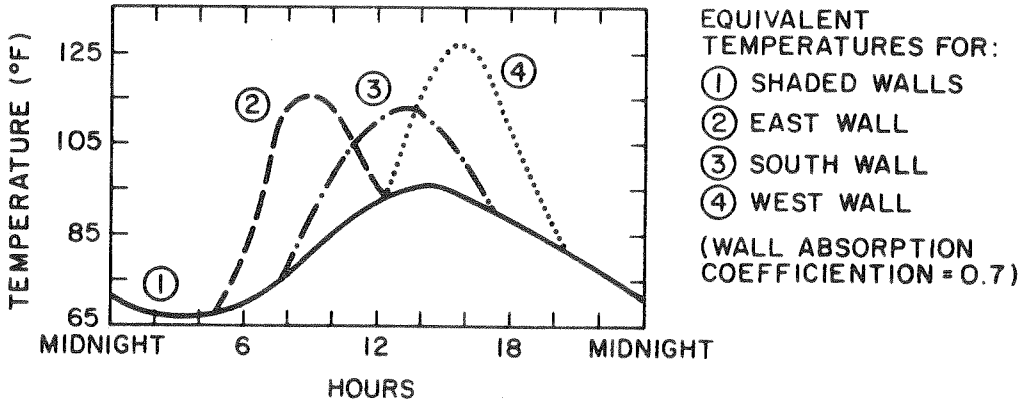

(c) VARIATIONS IN EQUIVALENT AIR TEMPERATURE DURING THE DAY

FIGURE 5 ENVIRONMENTAL BOUNDARY CONDITIONS FOR ROOFS AND WALLS

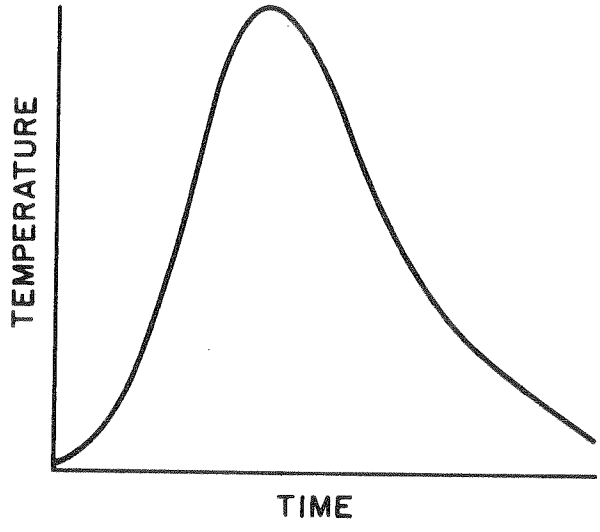

FIGURE 6 TEMPERATURE HISTORY OF A FIRE

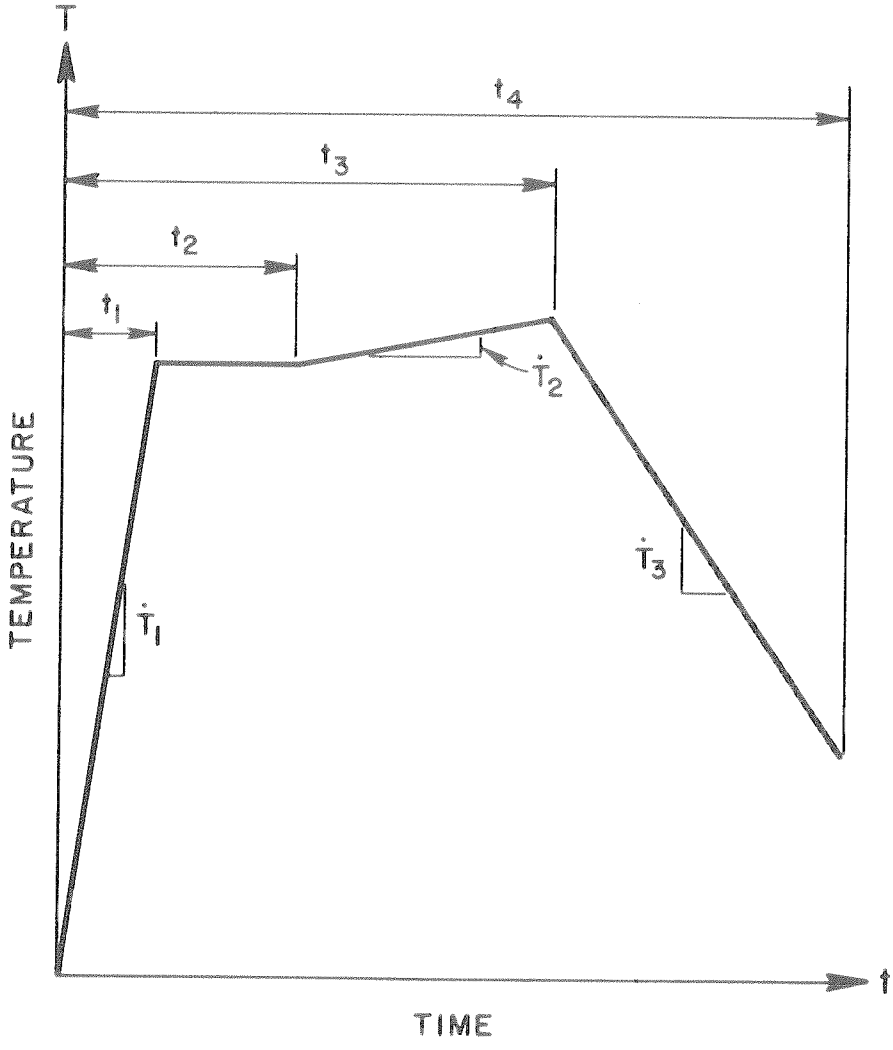

FIGURE 7 MULTILINEAR MODEL OF A PSEUDO-FIRE

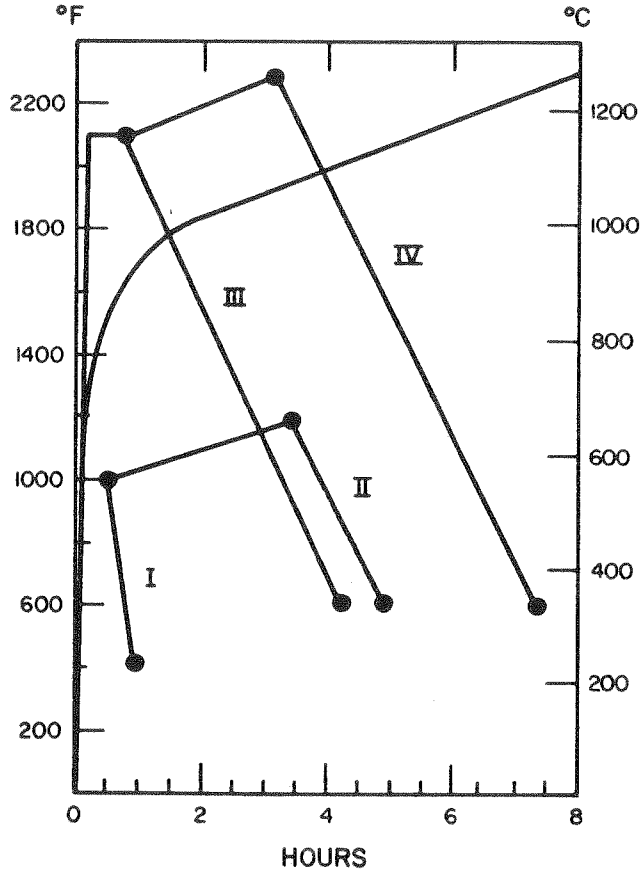

FIGURE 8 FOUR PROPOSED CATEGORIES OF DESIGN FIRE

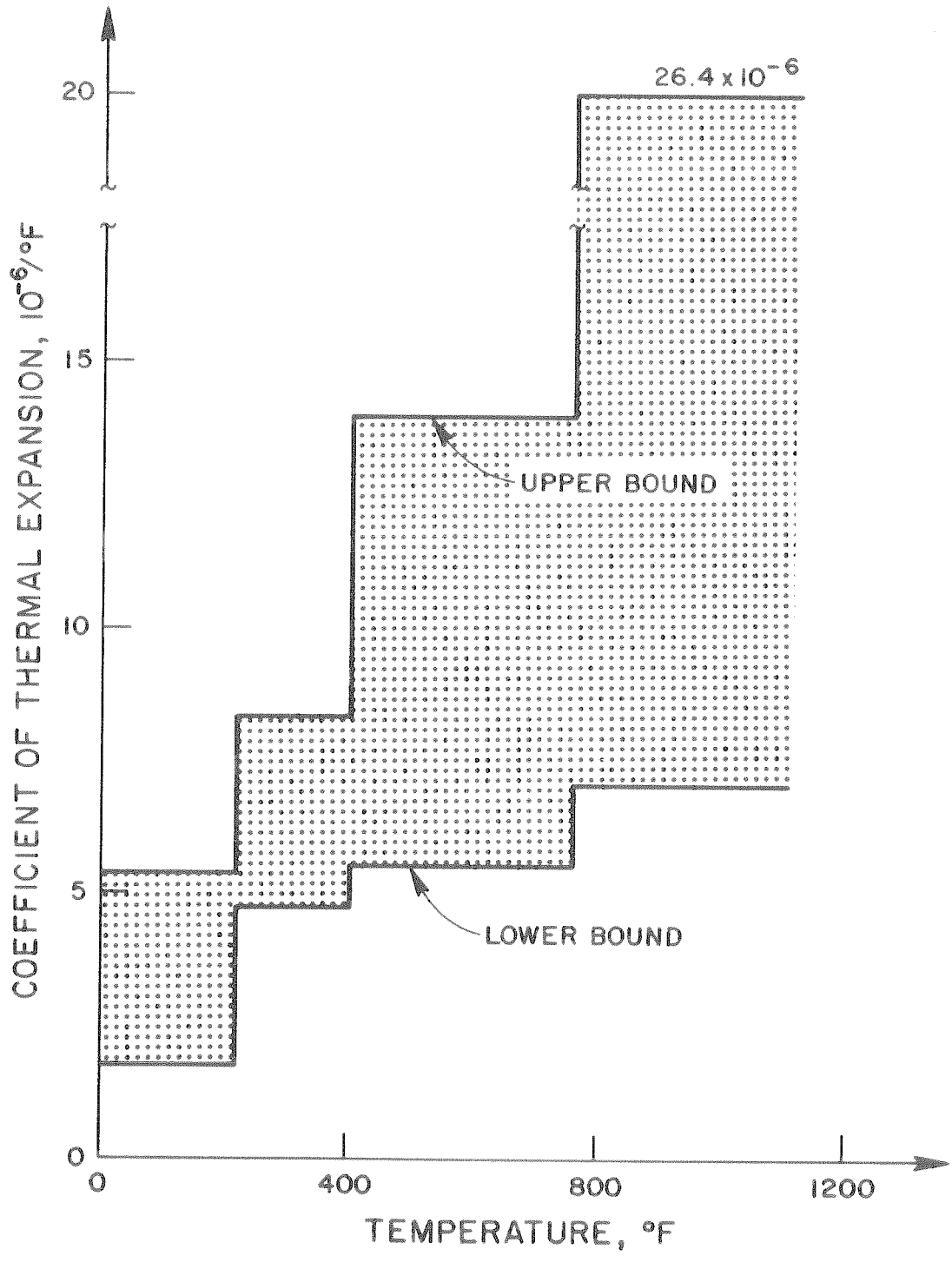

FIGURE 9A COEFFICIENTS OF THERMAL EXPANSION FOR CONCRETE

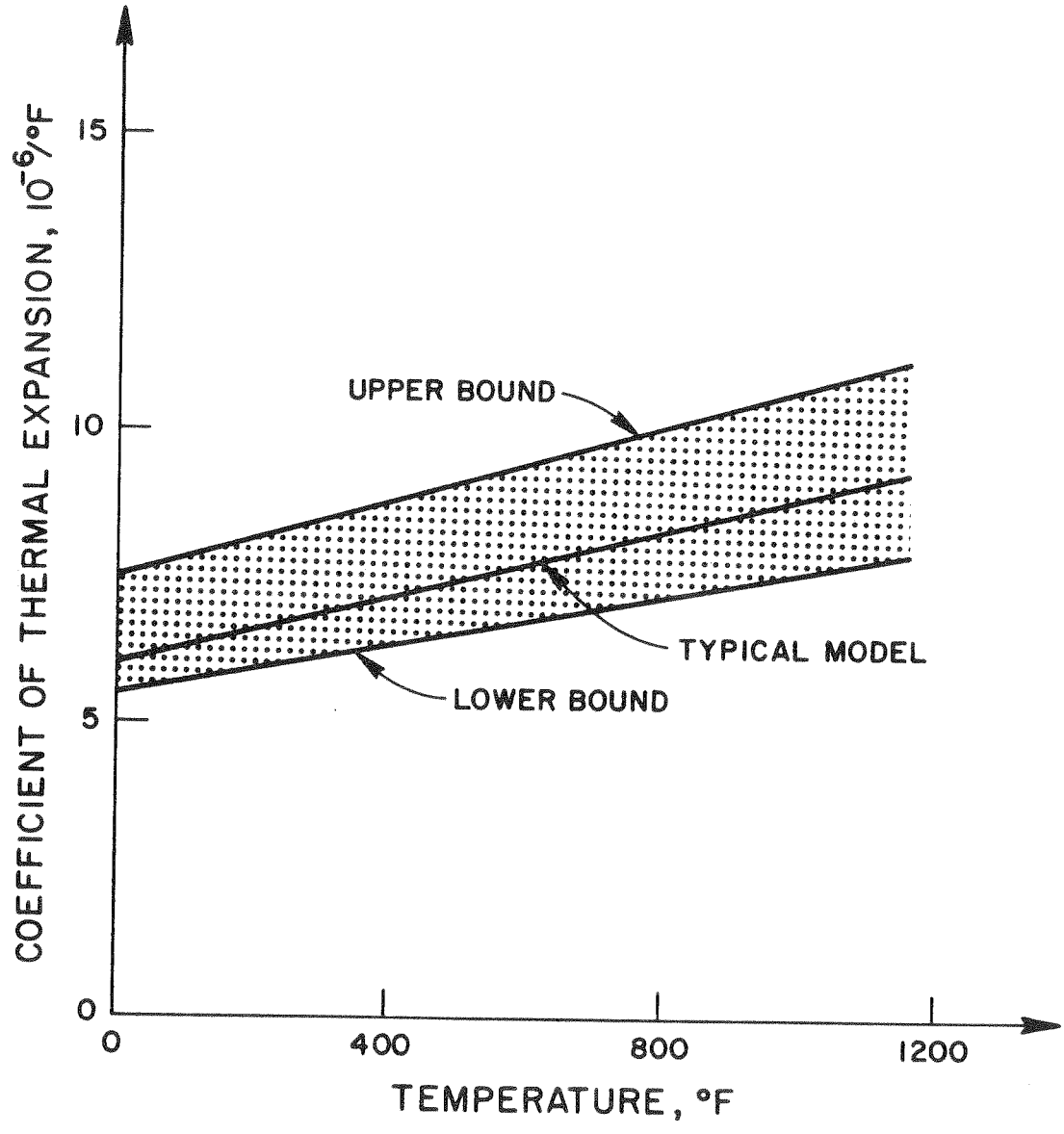

FIGURE 9B COEFFICIENTS OF THERMAL EXPANSION FOR STEEL

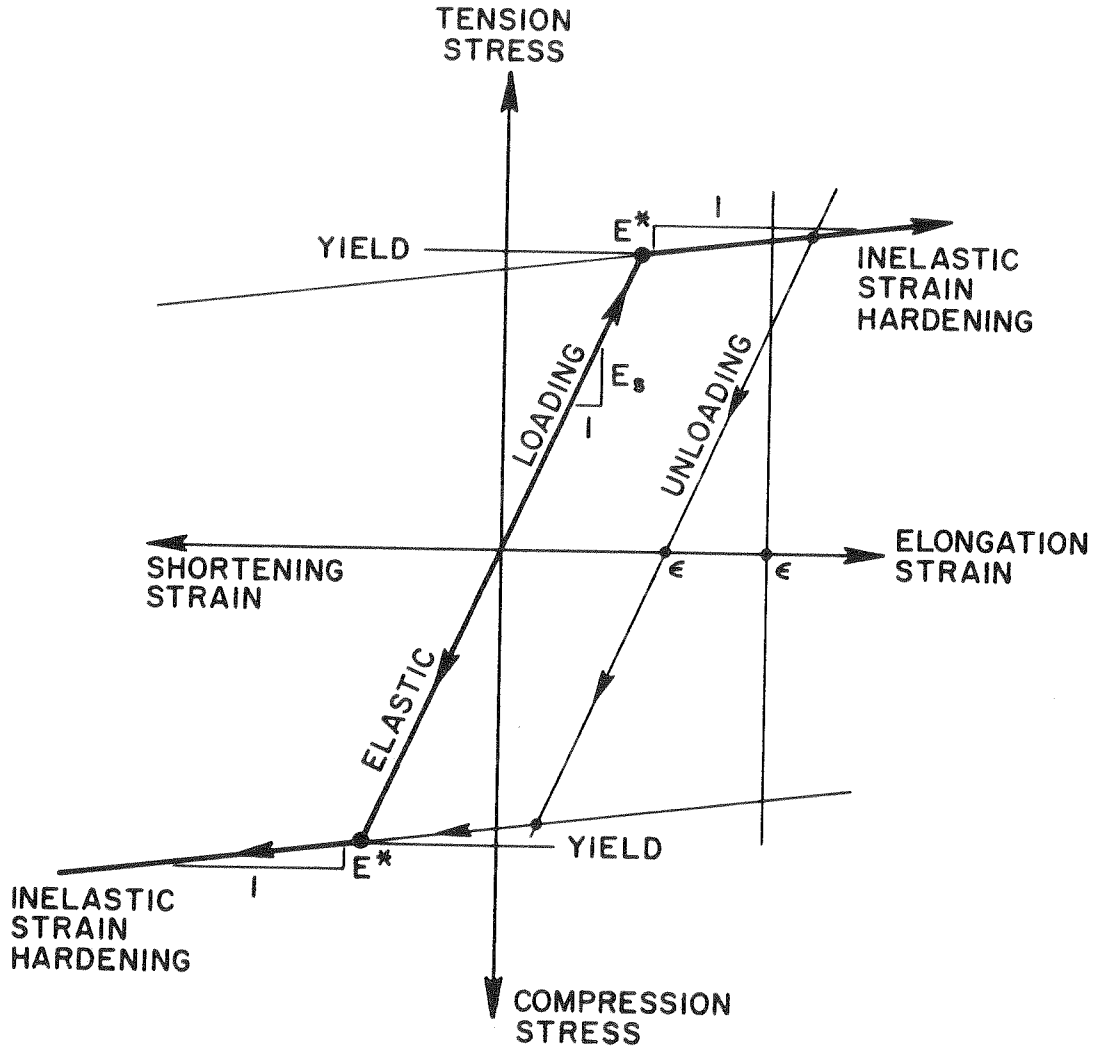

FIGURE 10 STRESS-STRAIN LAW FOR STEEL

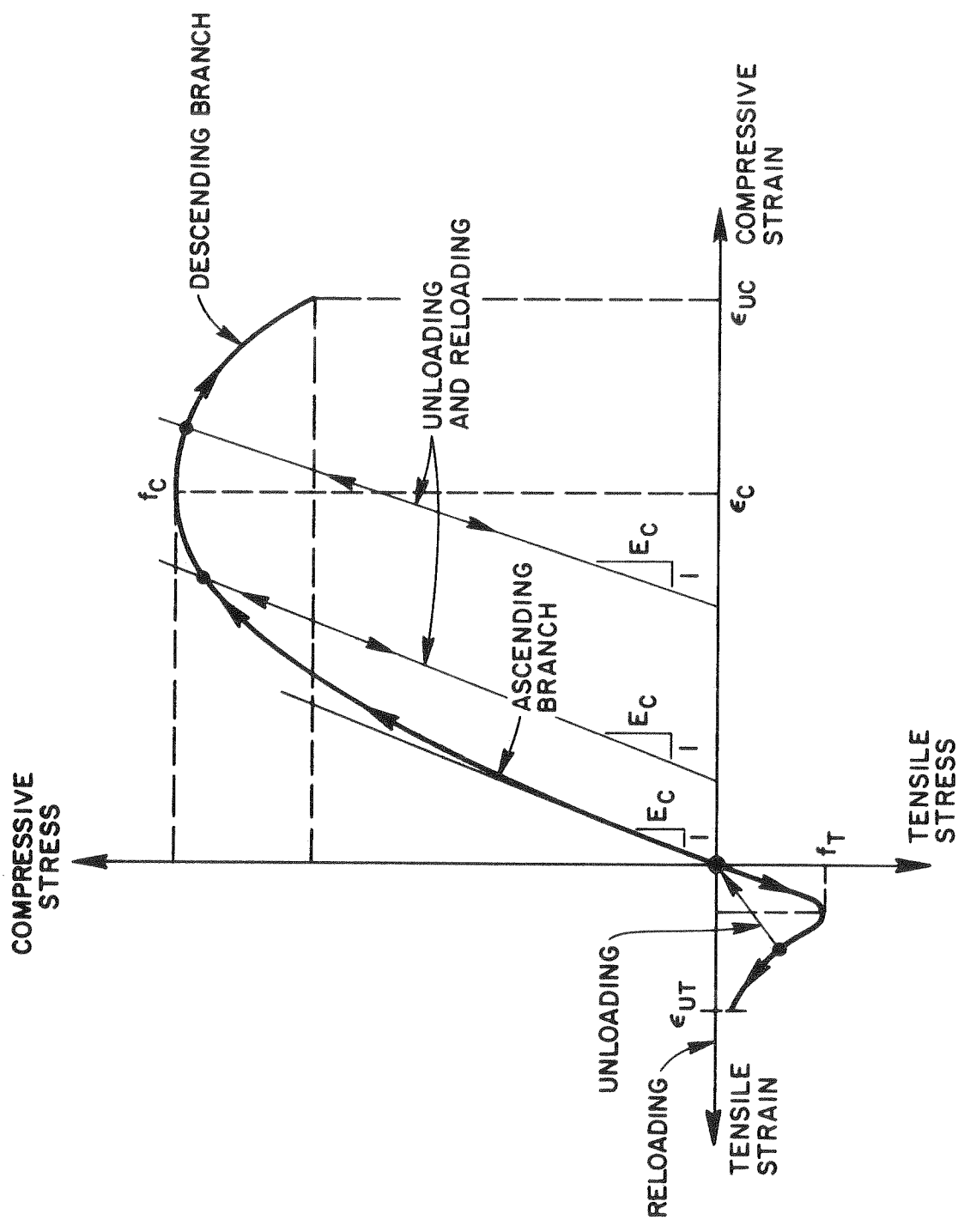

FIGURE 11 STRESS-STRAIN LAW FOR CONCRETE

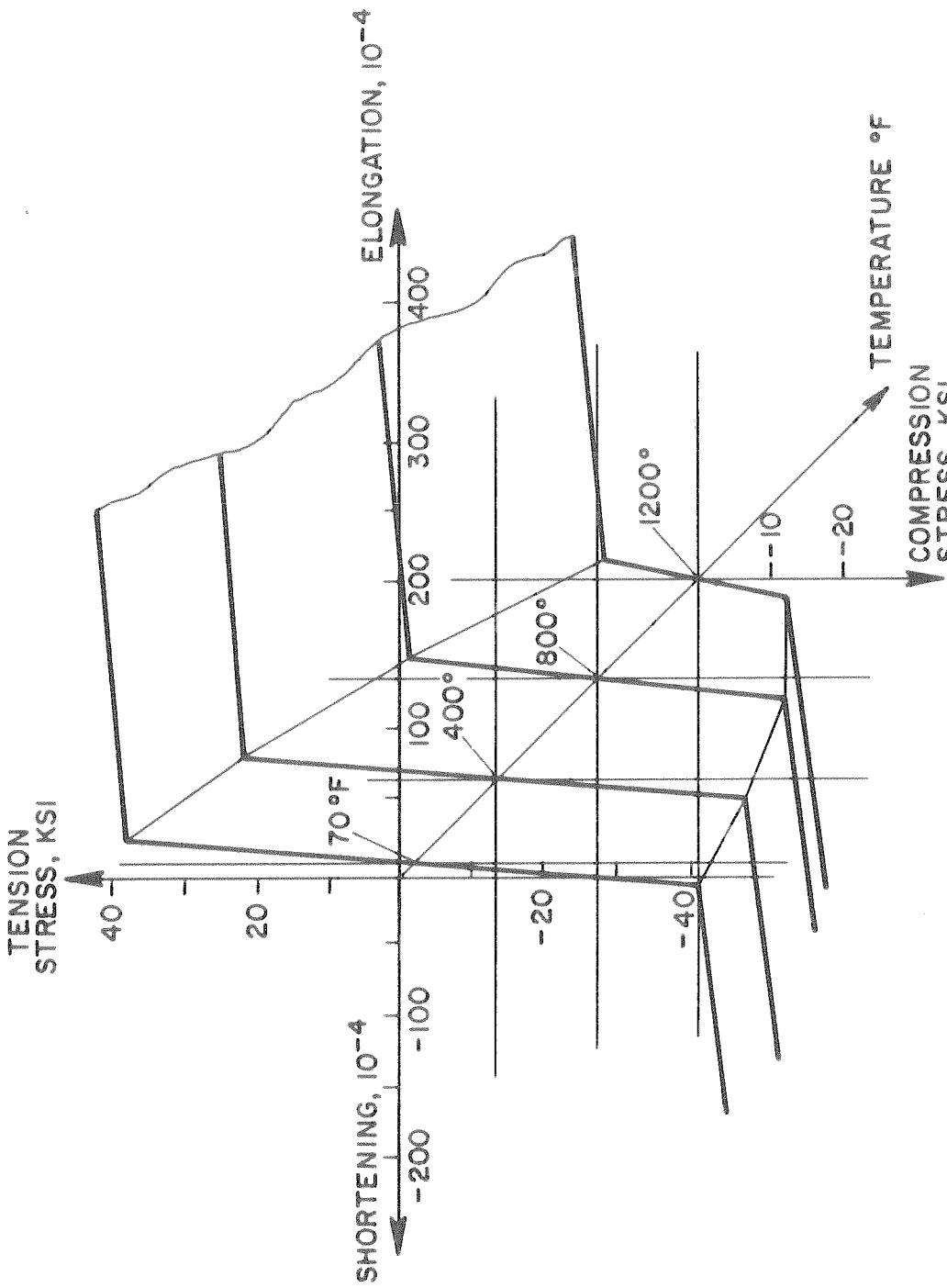

FIGURE 12 STRESS-STRAIN CURVES FOR STEEL AT ELEVATED TEMPERATURE

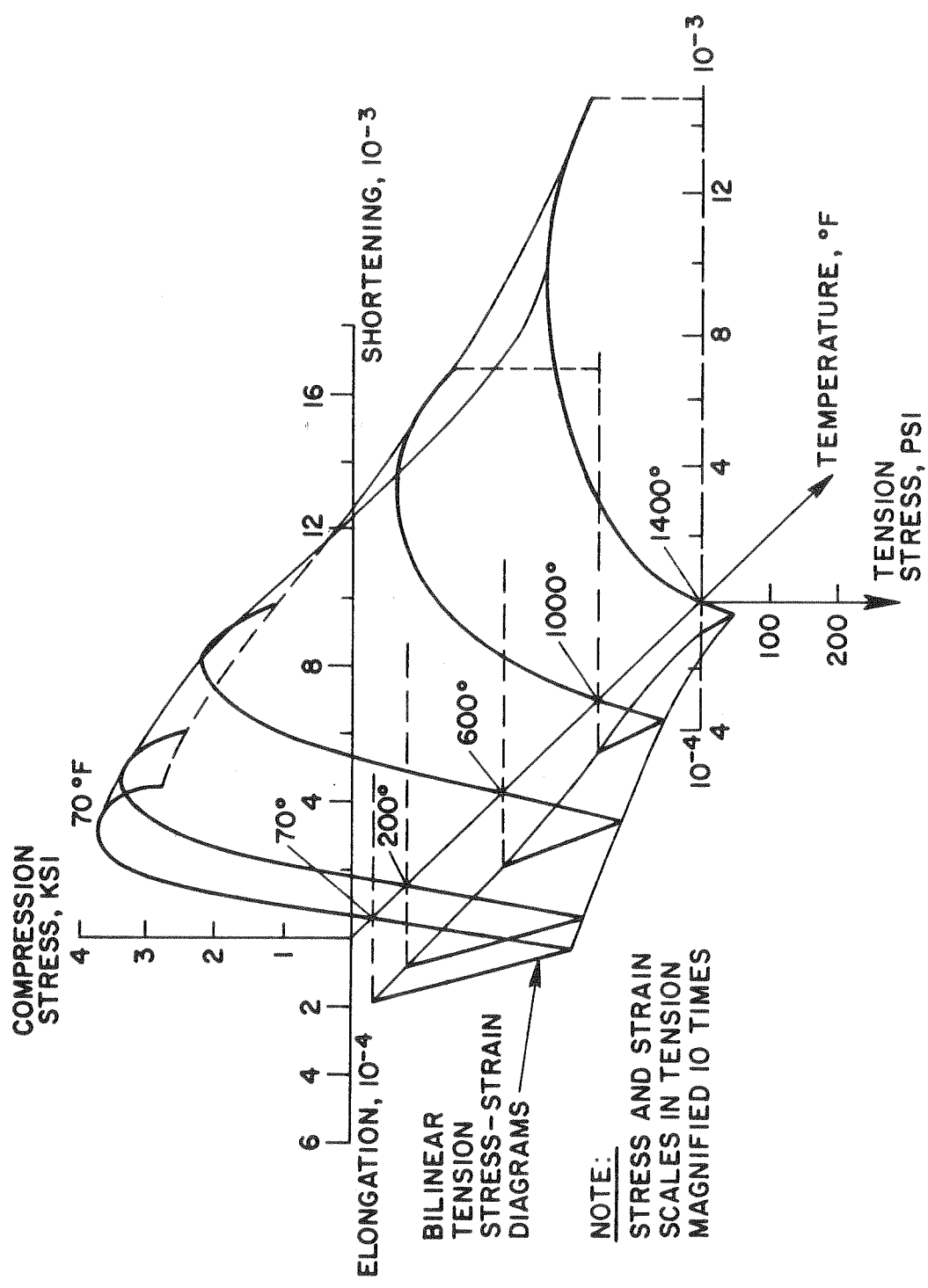

FIGURE 13 UNIAXIAL STRESS-STRAIN CURVES FOR CONCRETE AT ELEVATED TEMPERATURE

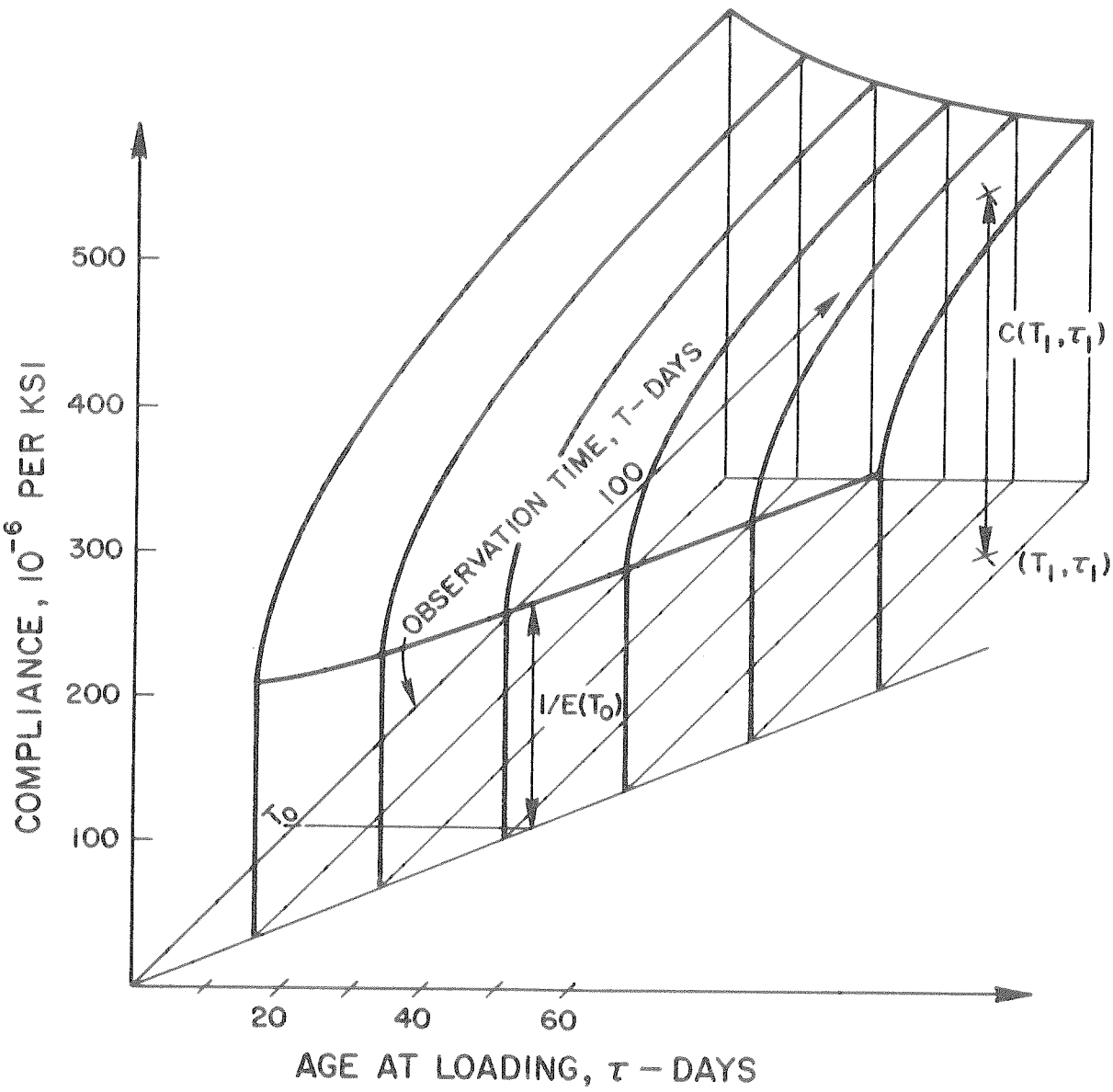

FIGURE 14 EFFECT OF AGING ON INSTANTANEOUS AND CREEP STRAINS

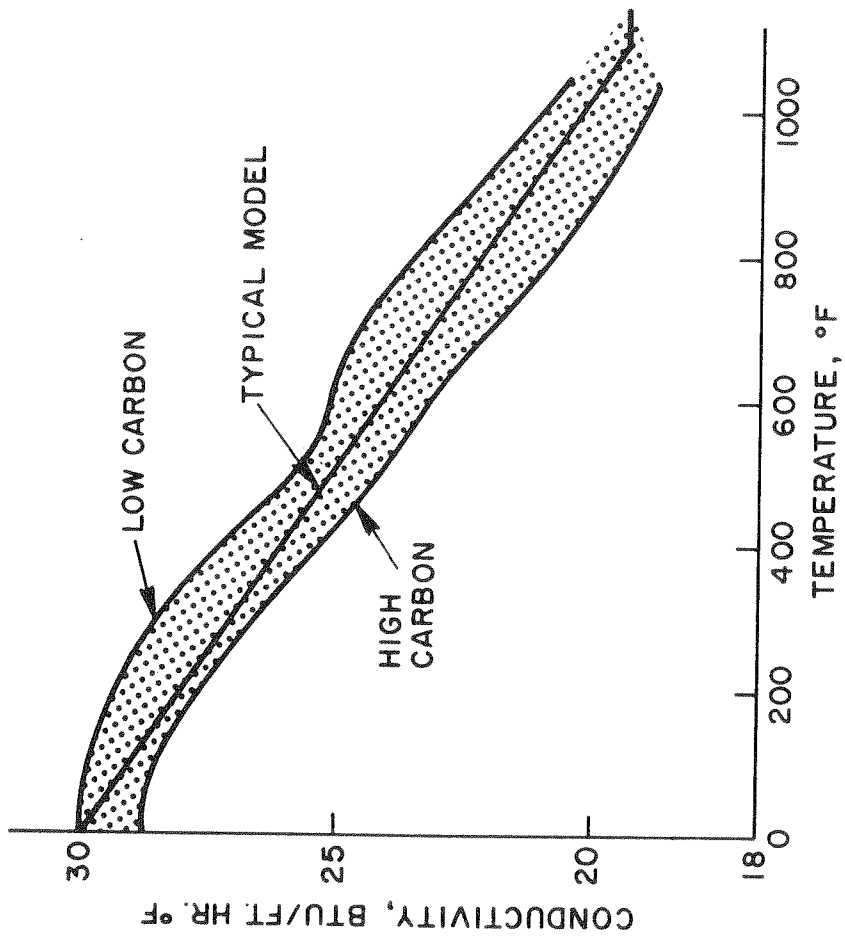

FIGURE 15A THERMAL CONDUCTIVITY - STEEL

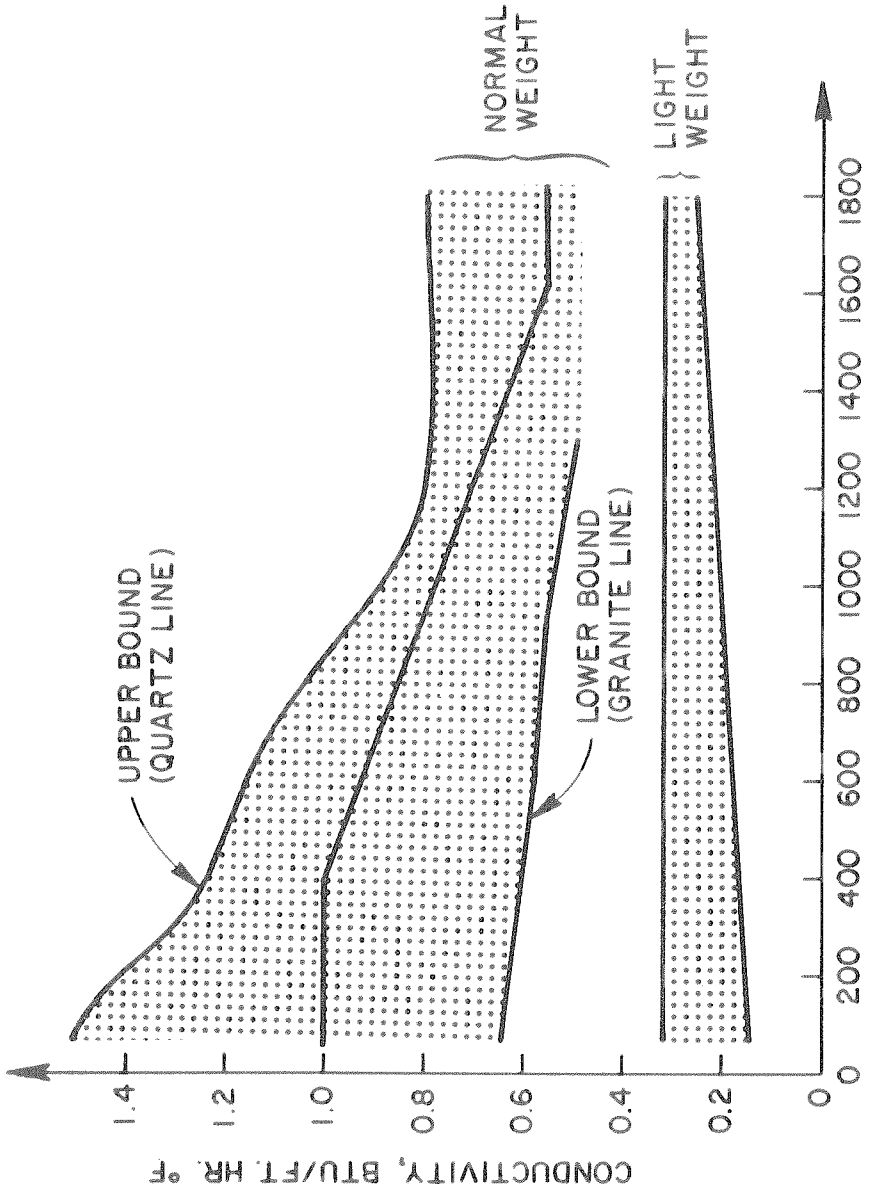

FIGURE 15B THERMAL CONDUCTIVITY - CONCRETE

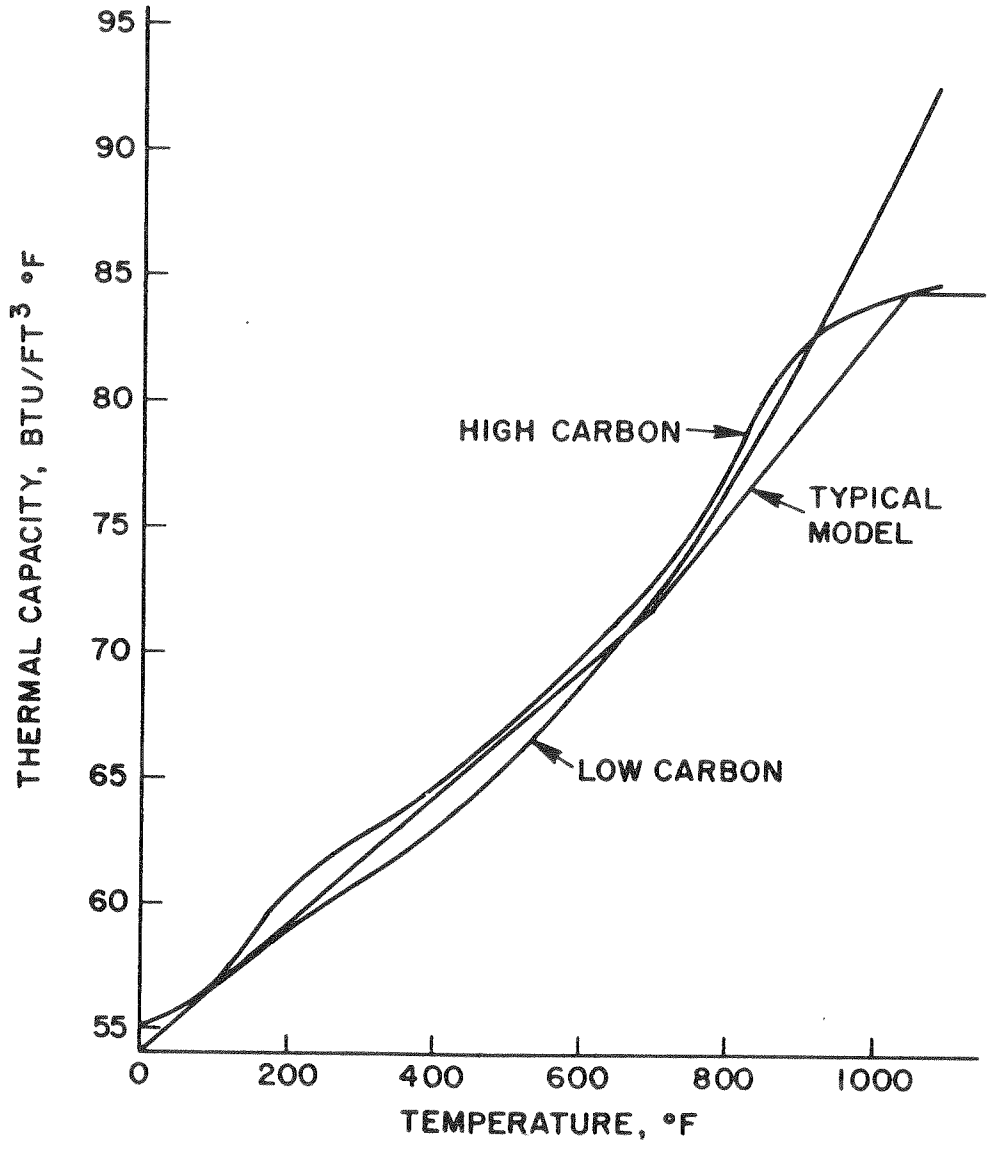

FIGURE 16A SPECIFIC HEAT - STEEL

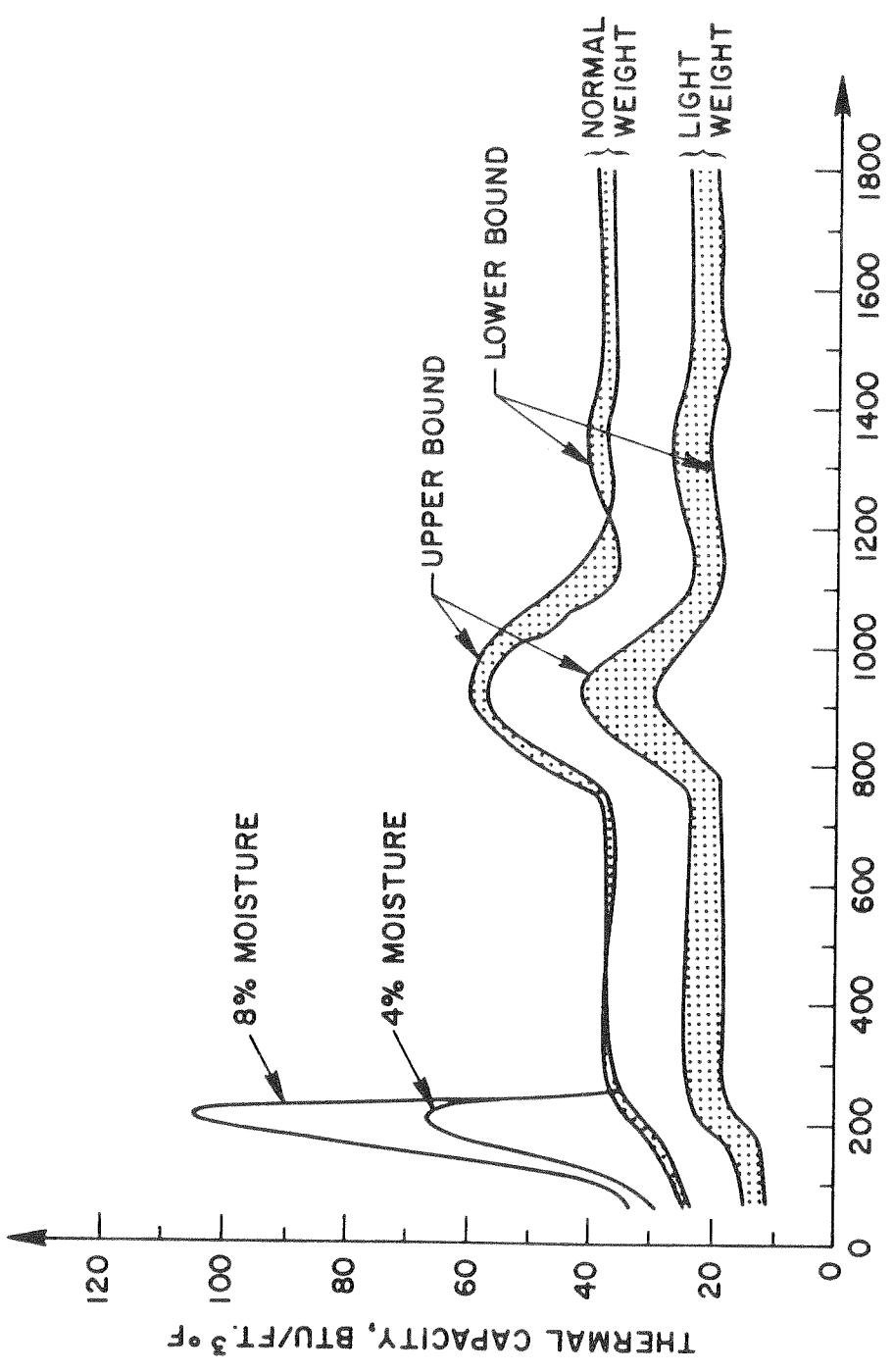

FIGURE 16B SPECIFIC HEAT - CONCRETE

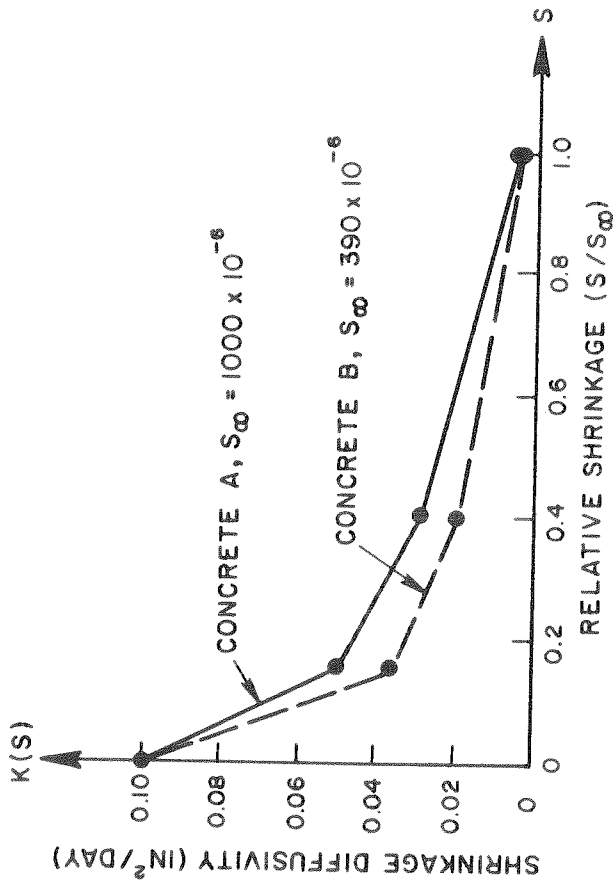

FIGURE 17 SHRINKAGE DIFFUSIVITY FOR CONCRETE

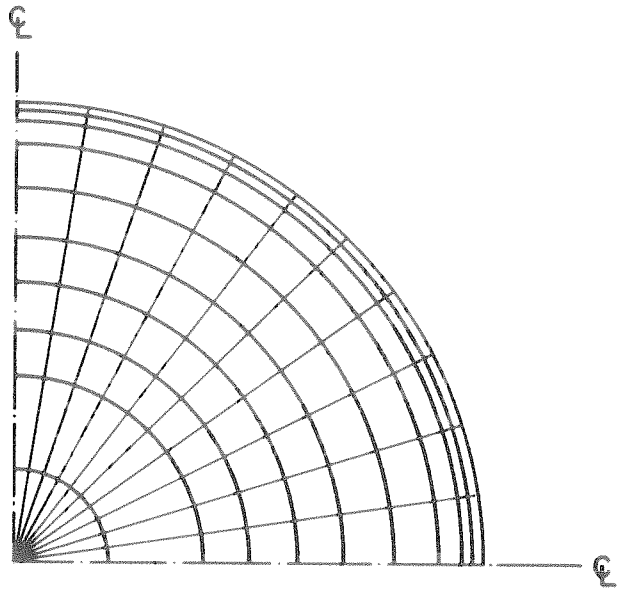

(a) DISCRETIZATION OF CYLINDER CROSS SECTION

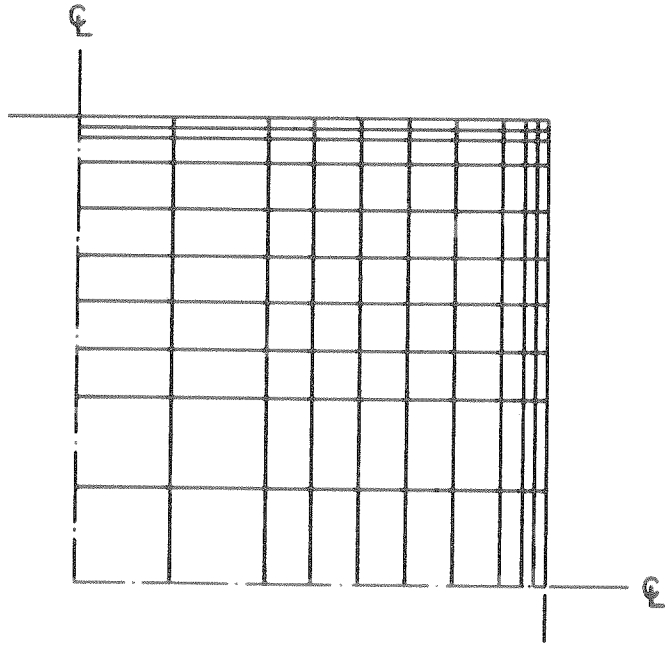

(b) DISCRETIZATION OF PRISM CROSS SECTION

FIGURE 18 CROSS SECTION DISCRETIZATION

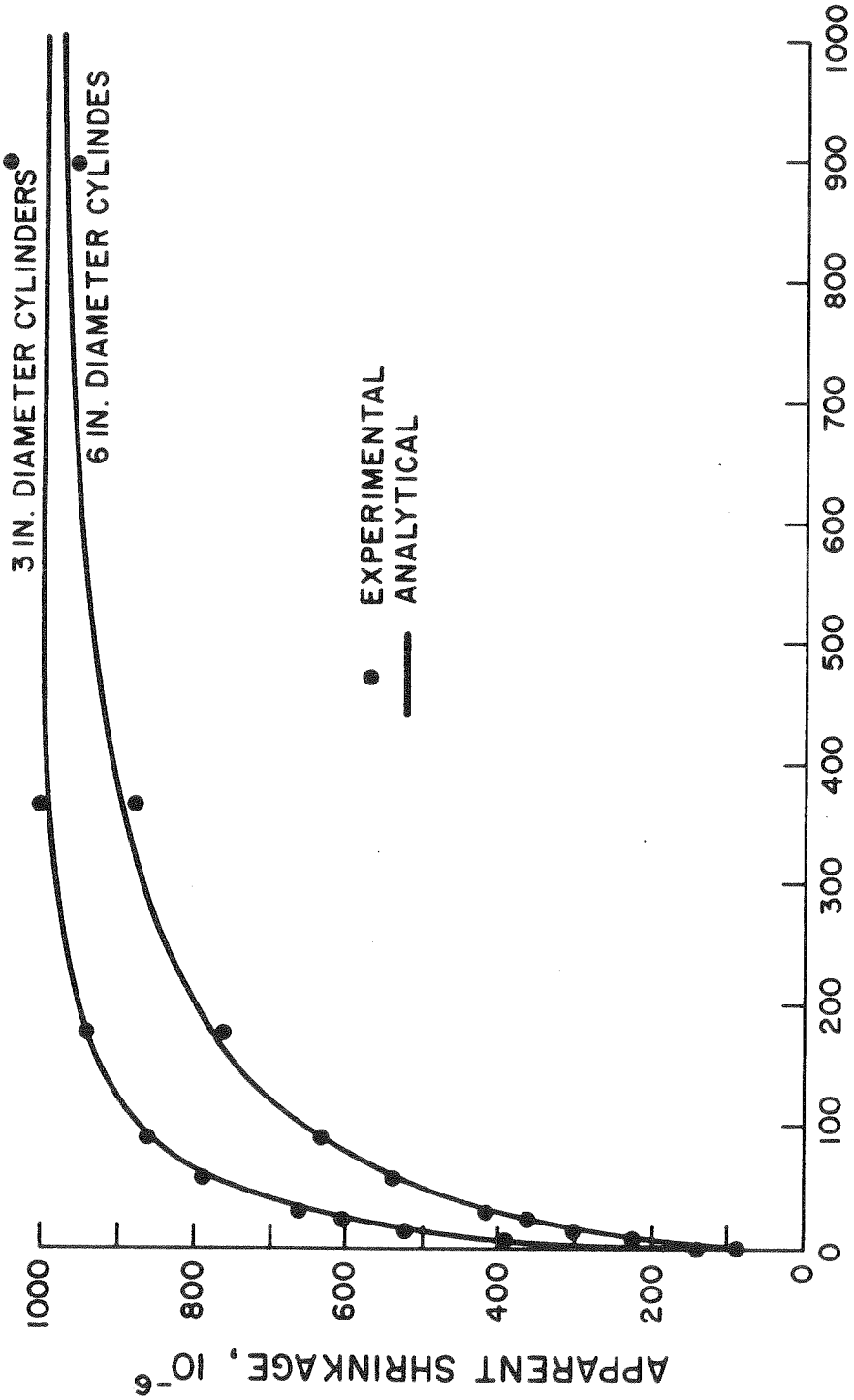

FIGURE 19 COMPARISON OF EXPERIMENTAL AND ANALYTICAL DATA - 3-INCH AND 6-INCH CYLINDERS

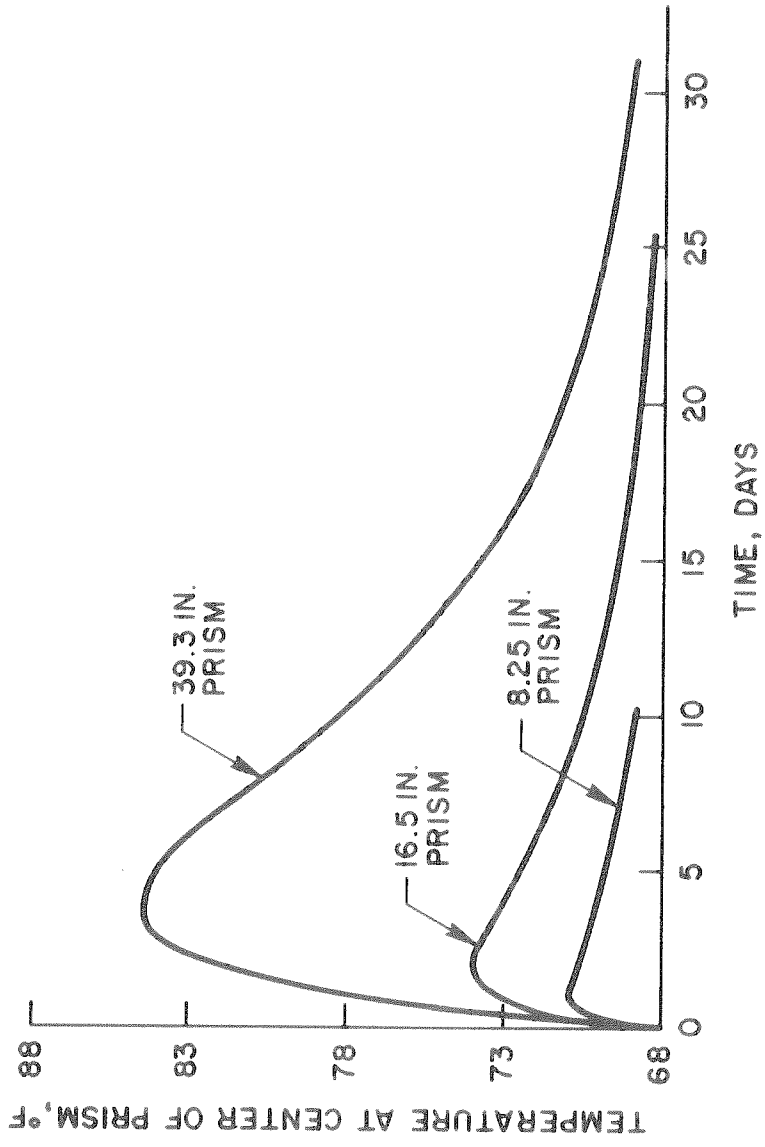

FIGURE 20 TEMPERATURE RISE DUE TO HEAT OF HYDRATION

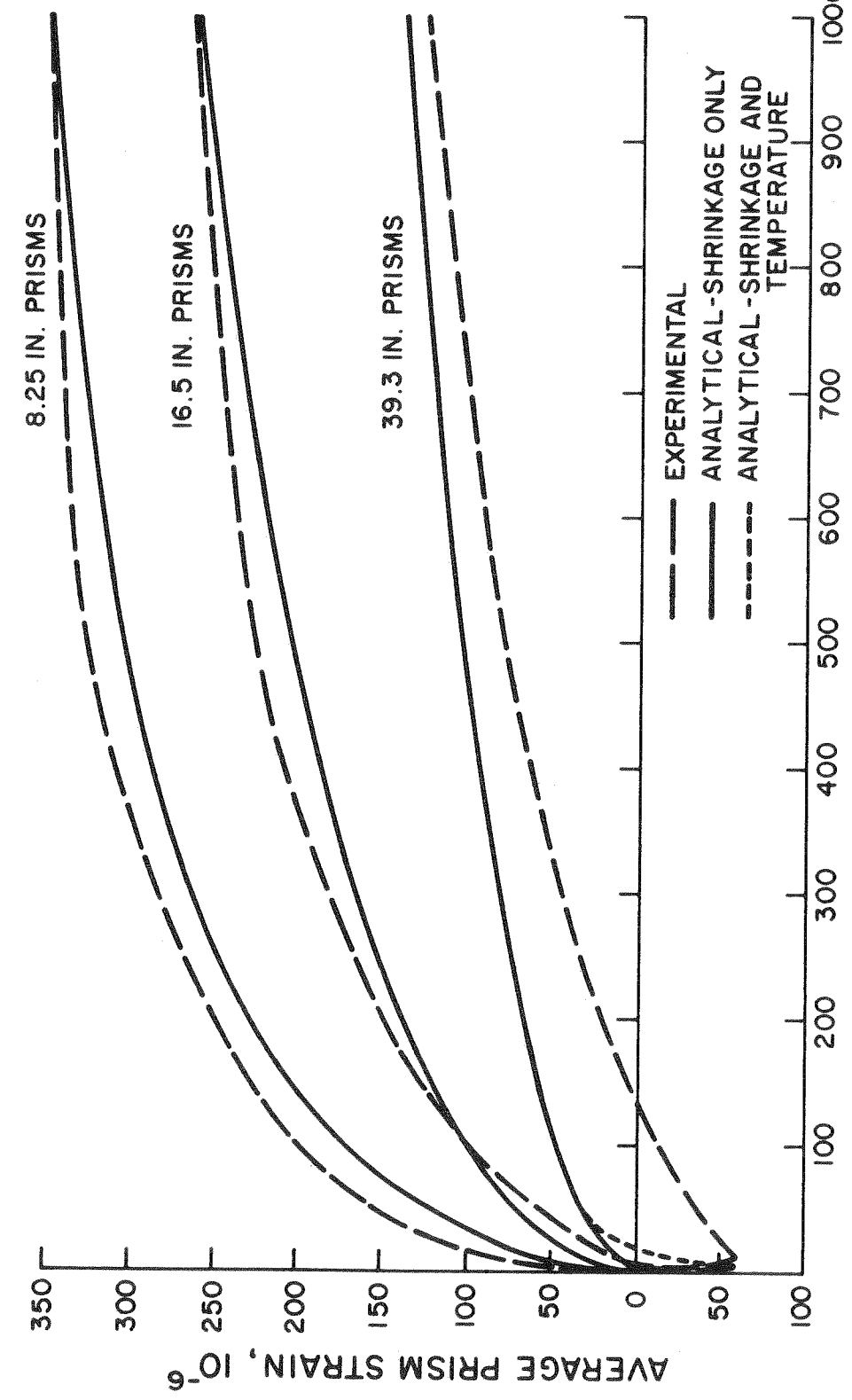

FIGURE 21 COMPARISON OF EXPERIMENTAL AND ANALYTICAL DATA - 8.25-INCH, 16.5-INCH, AND 39.3-INCH PRISMS

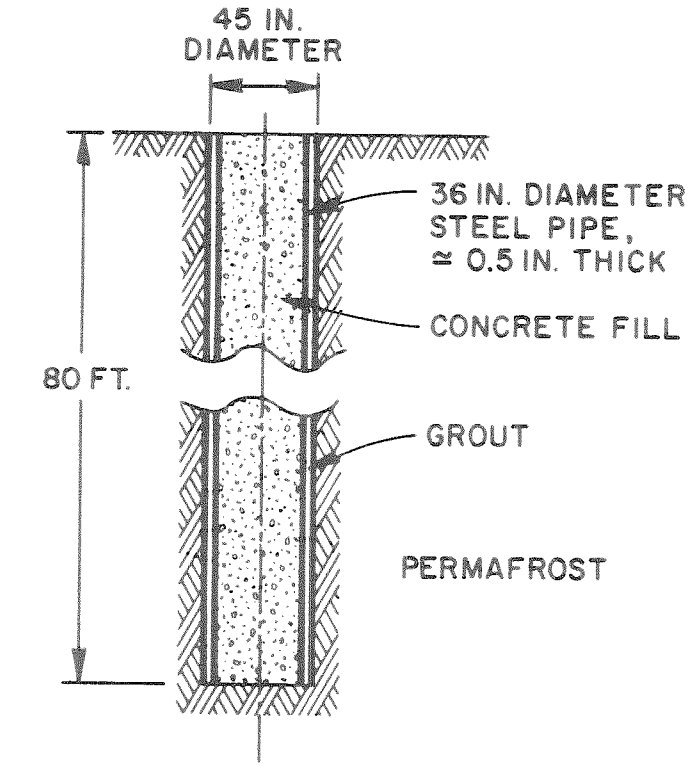

(a) CAISSON IN DRILLED PERMAFROST

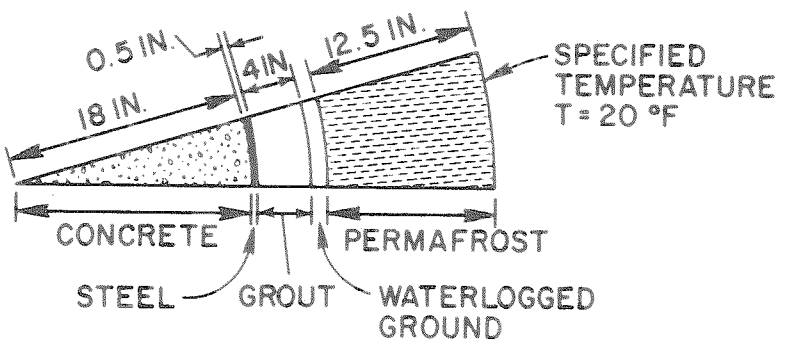

(b) GEOMETRIC IDEALIZATION

FIGURE 22 IDEALIZATION OF SAGAVARNIRKTOK CAISSON PROBLEM

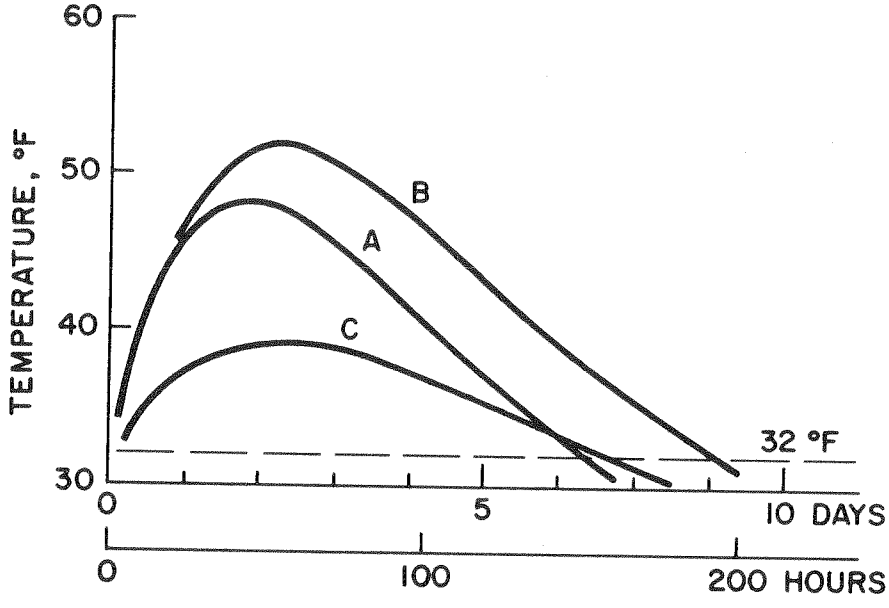

FIGURE 23 TEMPERATURE OF GROUT AT OUTER EDGE OF CAISSON

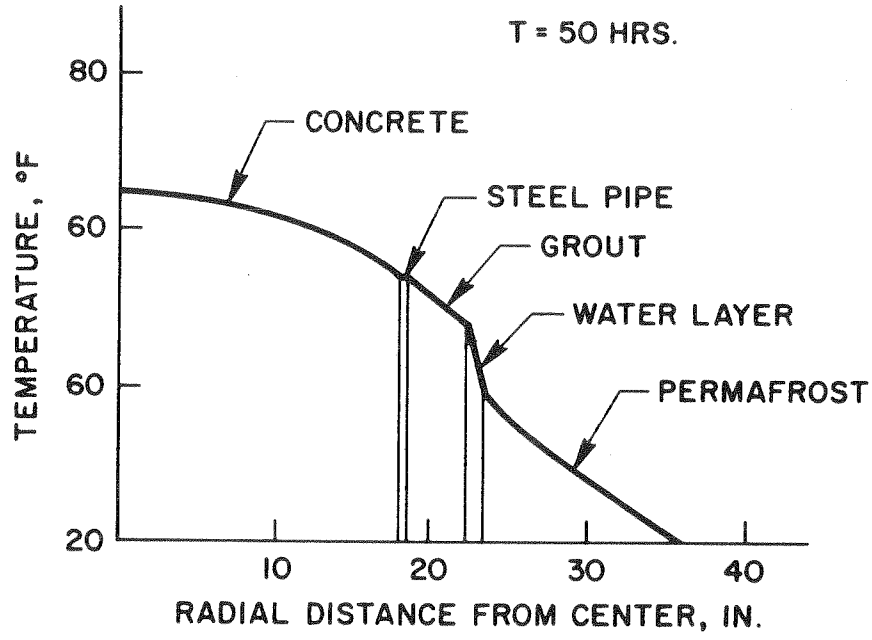

FIGURE 24 TEMPERATURE DISTRIBUTION IN CAISSON

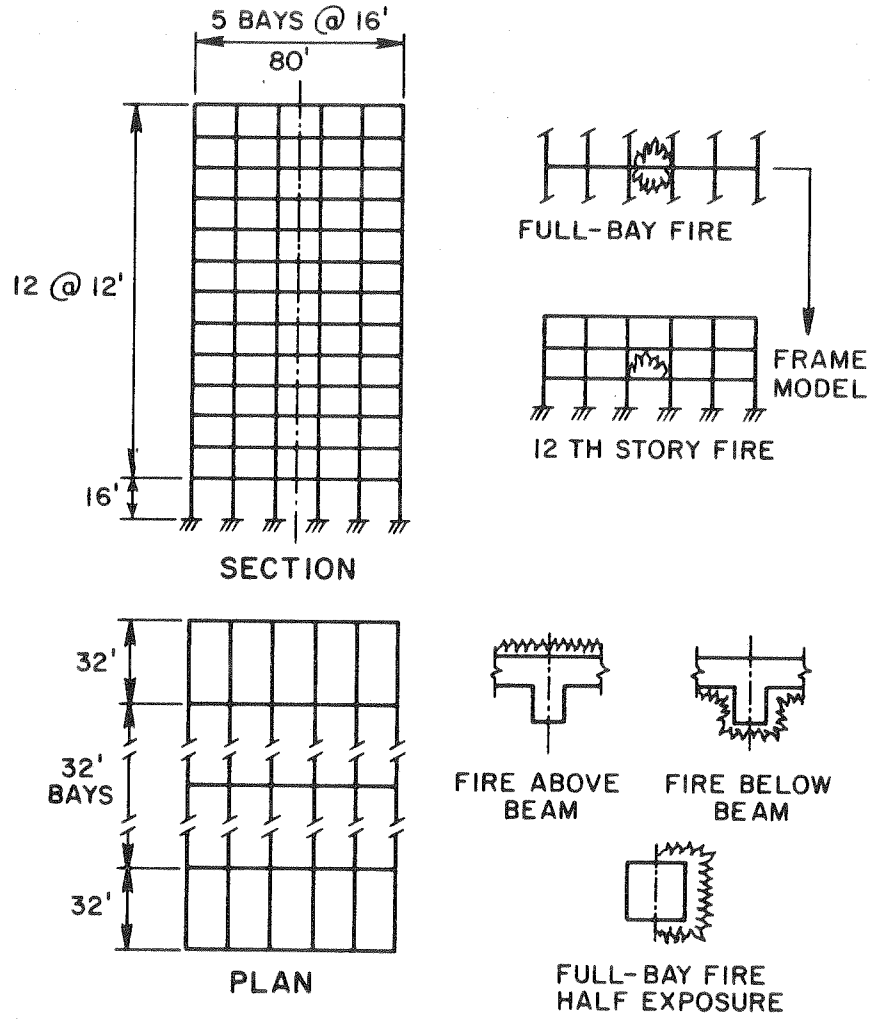

FIGURE 25 BUILDING PROTOTYPE, FIRE CONDITIONS, AND STRUCTURAL MODELS

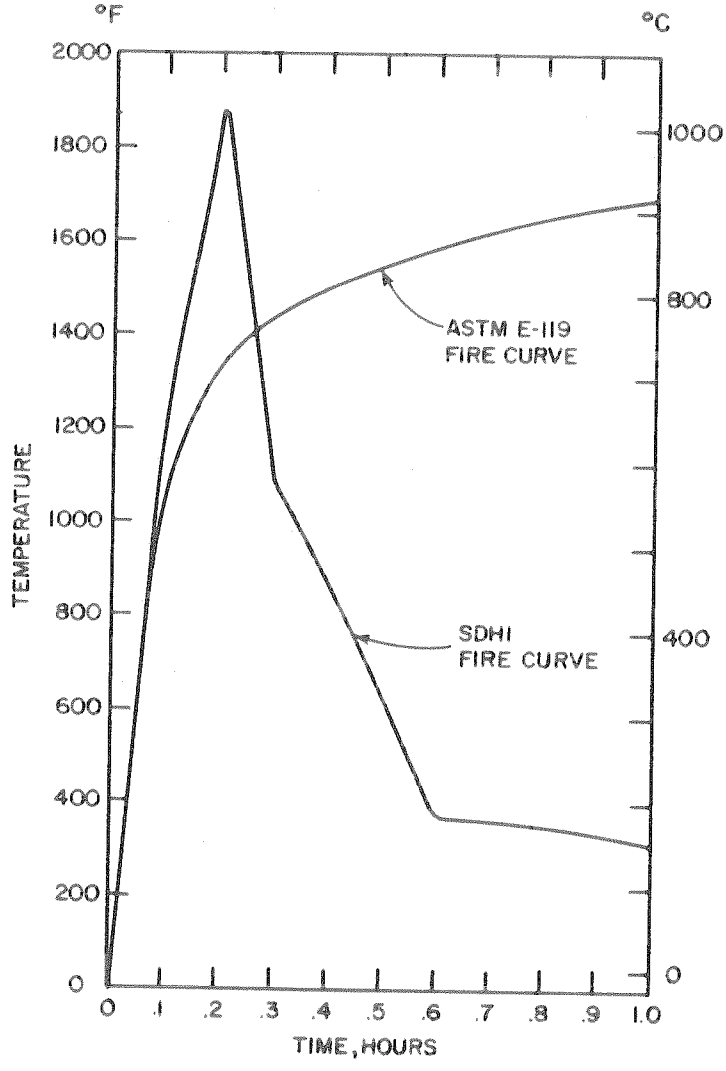

FIGURE 26 TIME-TEMPERATURE FIRE CURVES

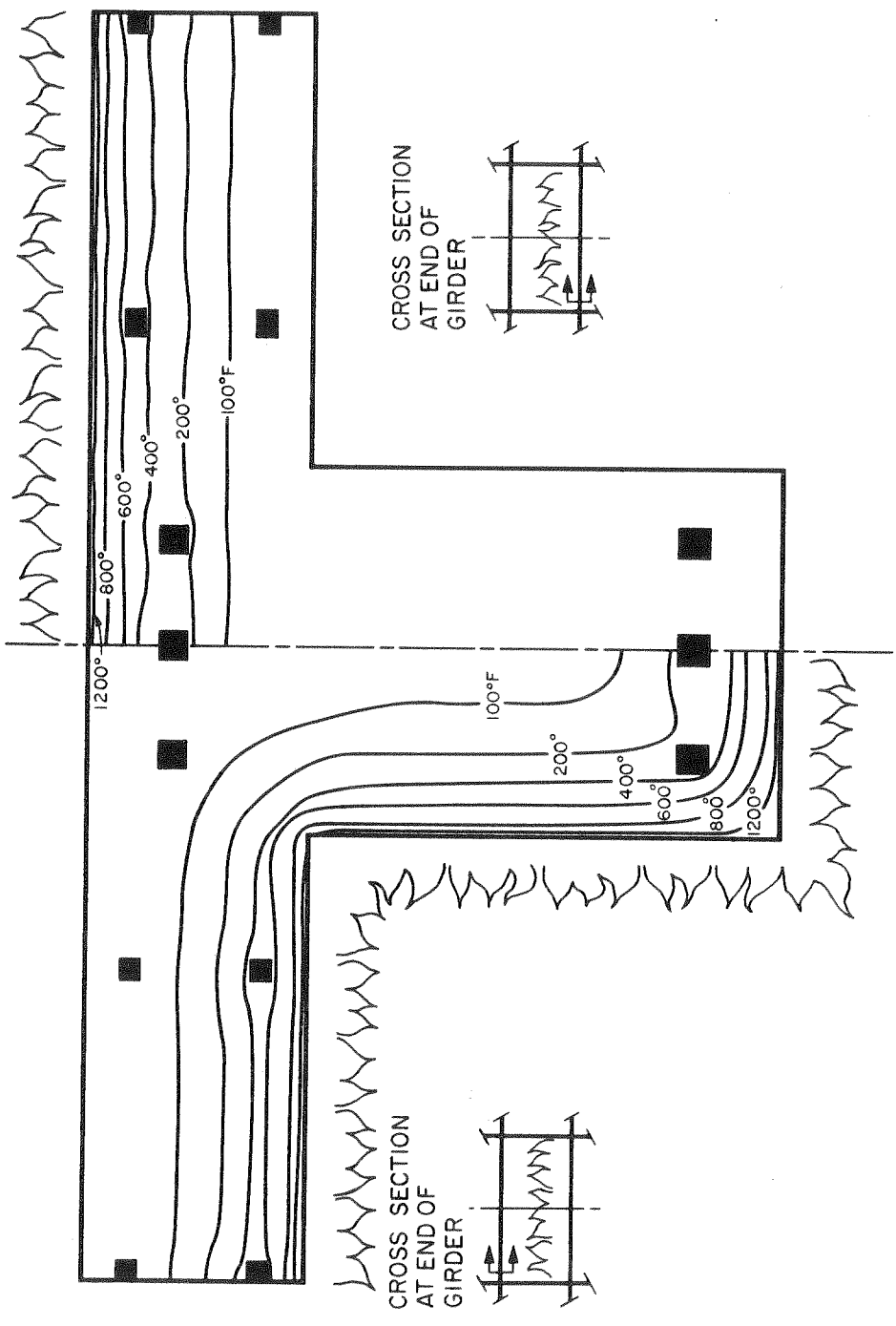

FIGURE 27 ISOTHERMS IN T-BEAM AFTER 0.5-HOUR ASTM FIRE

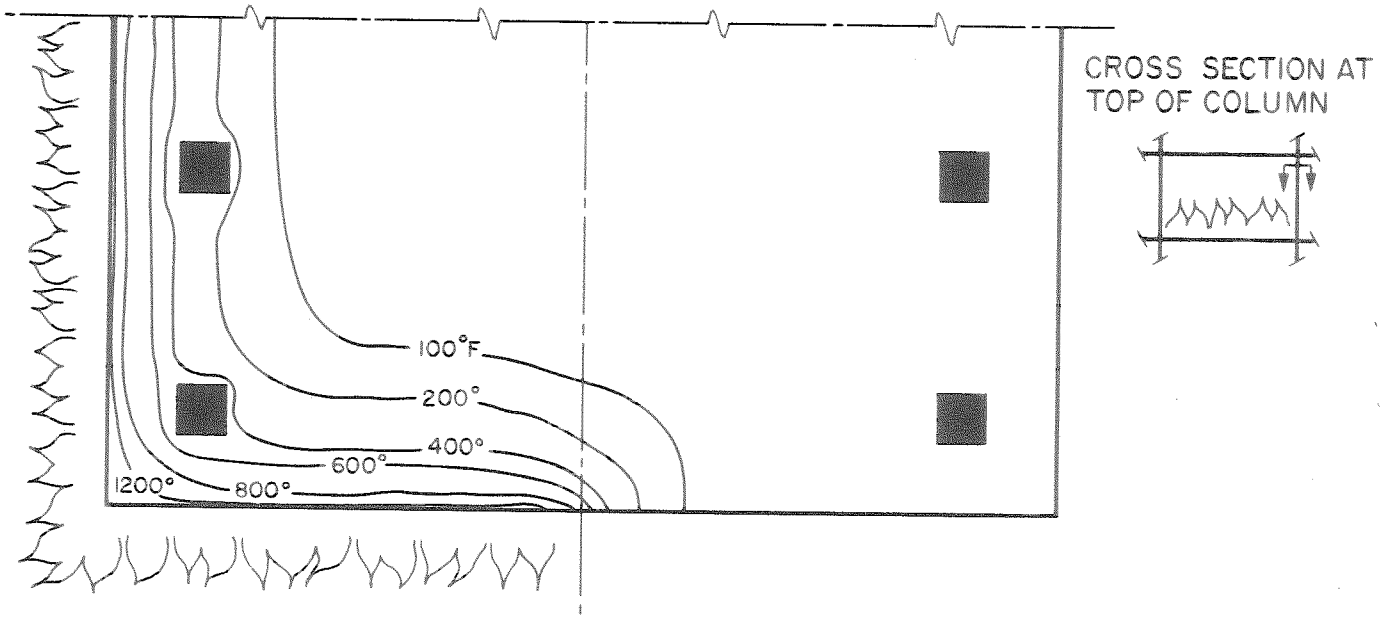

FIGURE 28 ISOTHERMS IN COLUMN AFTER 0.5-HOUR ASTM FIRE

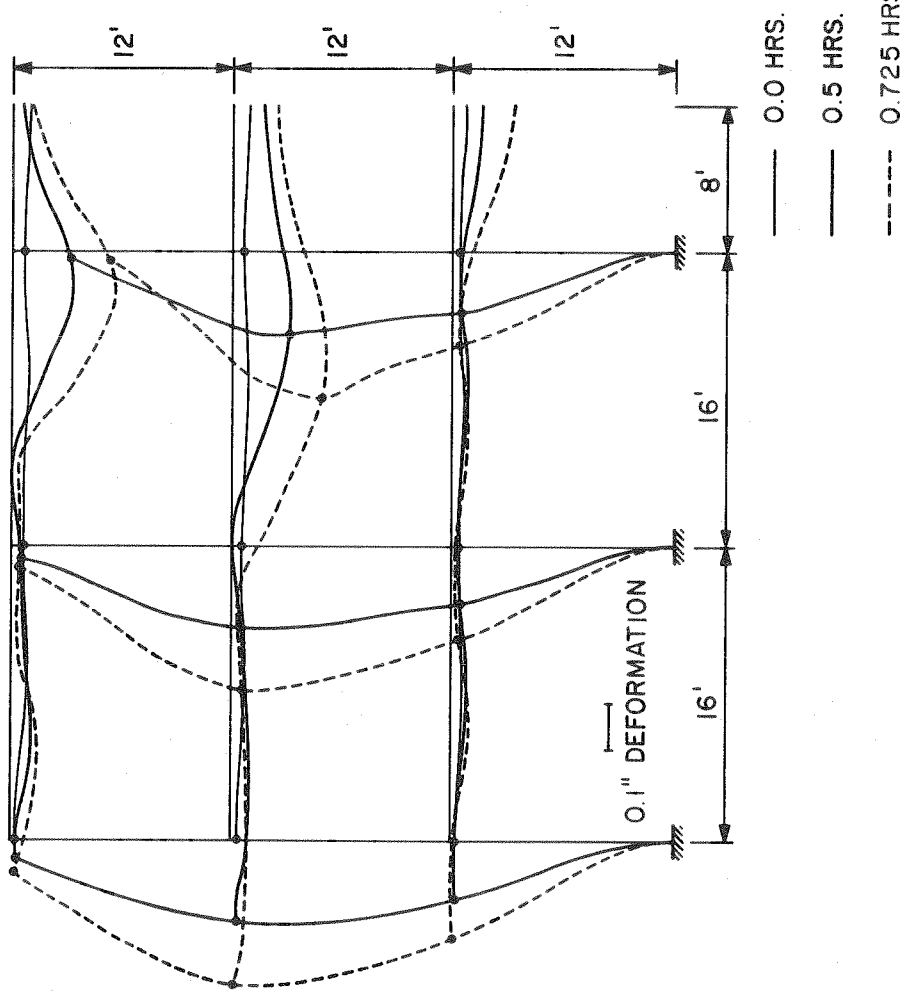

FIGURE 29 STRUCTURAL DEFORMATIONS DUE TO ASTM FIRE

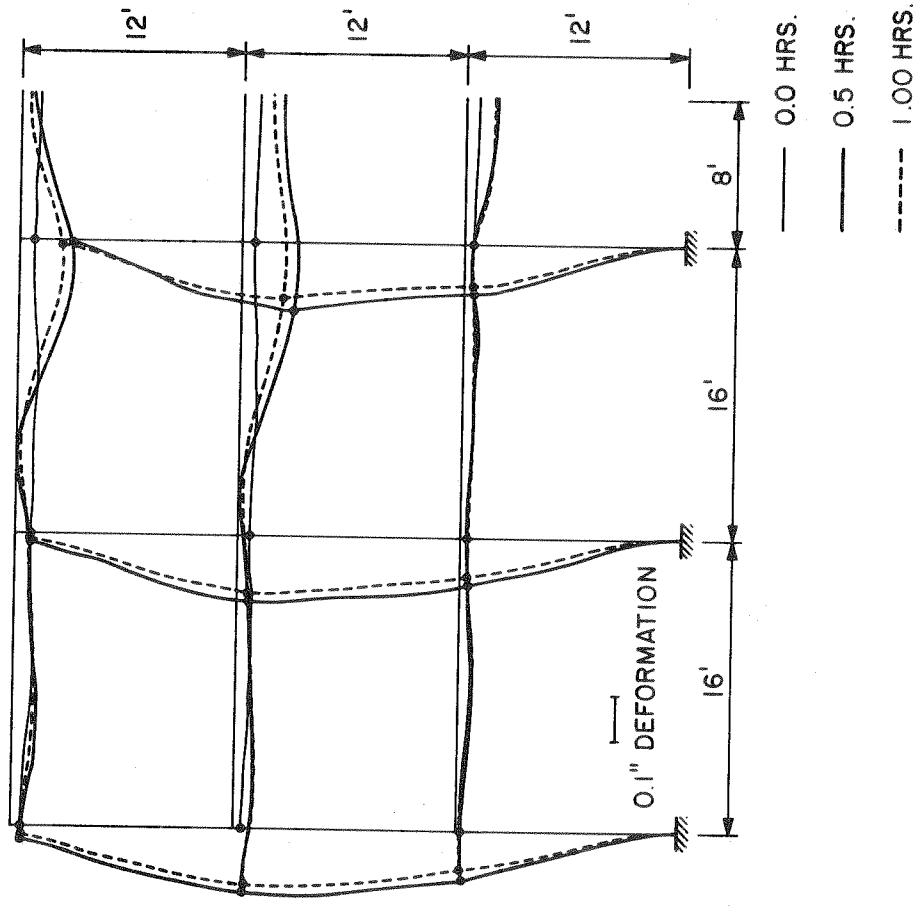

FIGURE 30 STRUCTURAL DEFORMATIONS DUE TO SDHI FIRE

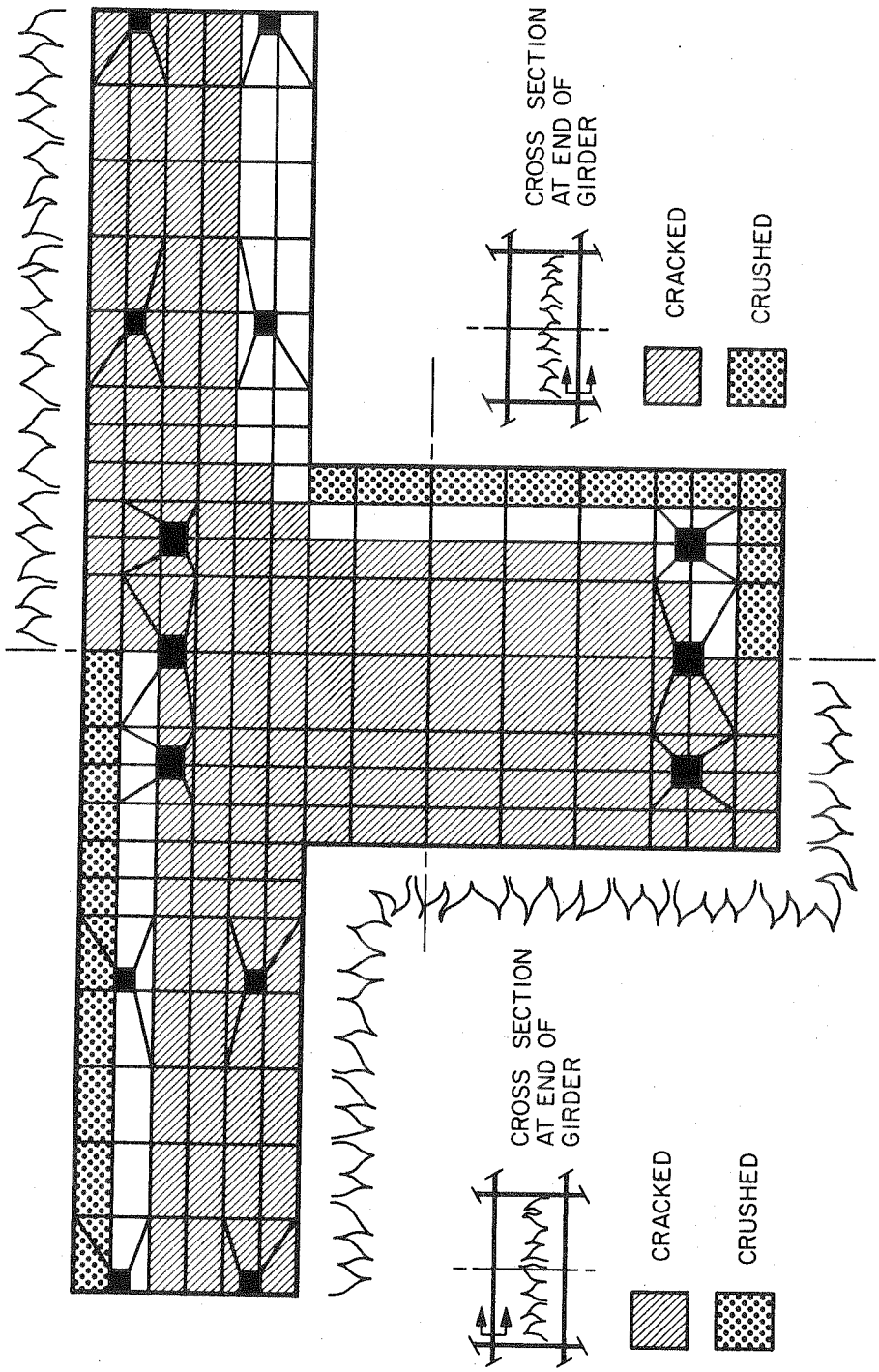

FIGURE 31 DEGRADATION PATTERN IN T-BEAM

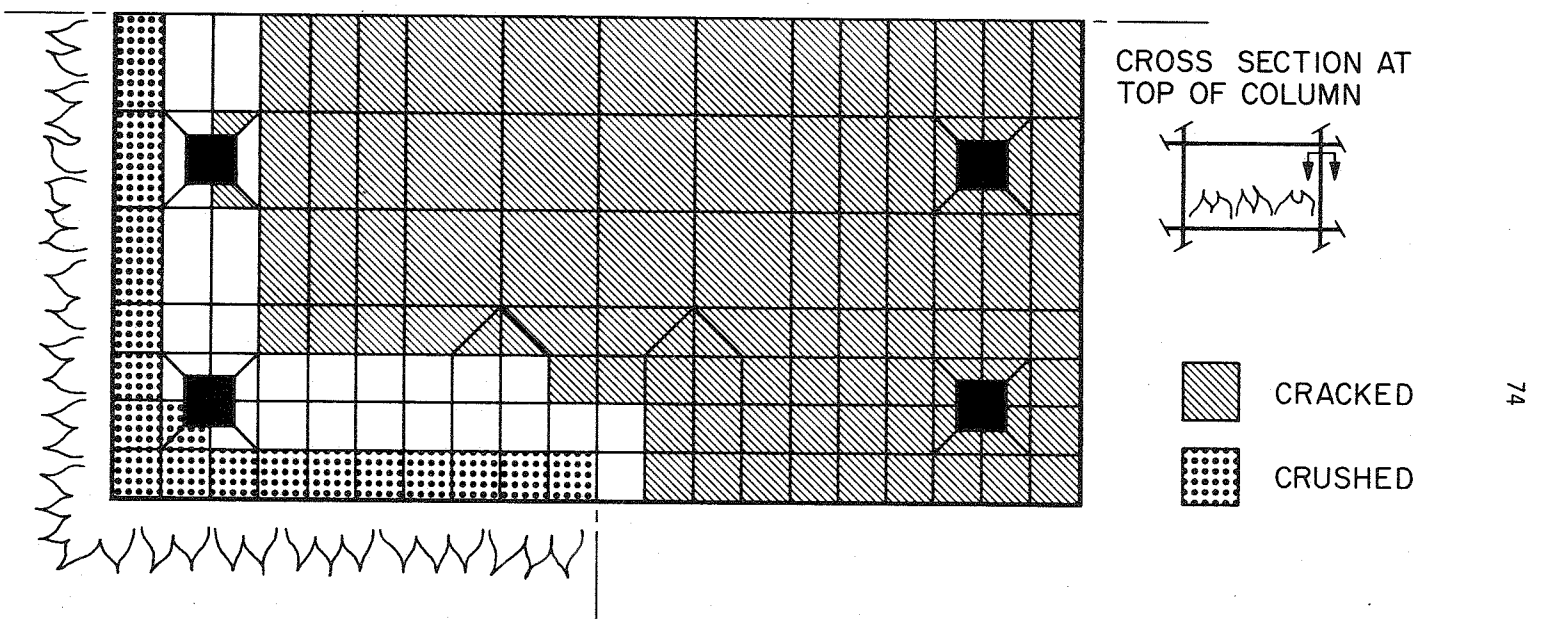

FIGURE 32 DEGRADATION PATTERN IN COLUMN